Fatigue Life Analysis of Welds in Conveyor Belts

Carl Larsson & Elias Jonasson

Avdelningen för Konstruktionsteknik
Lunds Tekniska Högskola
Lunds Universitet, 2026

Rapport TVBK-5315

Avdelningen för Konstruktionsteknik
Lunds Tekniska Högskola
Box 118
221 00 LUND

Division of Structural Engineering
Faculty of Engineering, LTH
P.O. Box 118
S-221 00 LUND
Sweden

Fatigue Life Analysis of Welds in Conveyor Belts

Analys av utmattningslivslängd för svetsar i transportband

Carl Larsson & Elias Jonasson

2026

Rapport TVBK - 5315
ISSN 0349-4969
ISRN: LUTVDG/TVBK - 26/5315 - SE

Master thesis
Supervisors: Professor Sebastian Thöns, Division of Structural Engineering, LTH
Jimmy Carlsson, MSc, JBT Marel.
Göran Gramby, MSc, JBT Marel.
8th June 2026

Abstract

This report studies fatigue in welded steel structures of a conveyor belt using the finite element method (FEM) together with hand calculations based on nominal stress. Three methods were used to evaluate stress at critical locations, the nominal stress method, the hot-spot method, and the effective notch stress method. Detailed FEM models were created where weld geometry and critical stress concentrations were included through local mesh refinement in critical regions.

Several load systems were analysed to represent different operating conditions of the conveyor belt. Parameter studies were also performed to evaluate how variations in weld size and structural configuration affect the fatigue life. The results show differences between the evaluated methods. The effective notch method predicts higher local stress levels, while the hot-spot method describes structural stress concentrations and the nominal stress method mainly represents global stress effects.

The results indicate that local geometric variations and weld design have a strong influence on fatigue performance. Increasing the weld size reduces the stress levels and improves the predicted fatigue life.

Different material models were also analysed. A bilinear isotropic hardening model was performed to capture the plastic deformation of the structure. The resulting deformed geometry was then used as the basis for a linear stress analysis. These analyses resulted in a lower predicted fatigue life compared to the analyses using only a linear elastic material model. Analyses including large rotation effects were also performed, but these did not lead to any significant differences in fatigue life.

Overall, the evaluated methods describe different stress fields in welded structures. The predicted stress levels and fatigue life depend on both the modelling approach and the weld geometry. This affects the choice of a suitable fatigue assessment method.

Acknowledgements

This project was conducted at the Division of Structural Engineering in collaboration with JBT Marel and marks the conclusion of the five years of studies at Lund University of Technology.

We would like to express our sincere gratitude to our supervisors at JBT Marel, Jimmy Carlsson and Göran Gramby, for their expertise, guidance, and continuous support throughout this project. Their valuable insights and constructive feedback have been very important for the successful completion of this work. We would also like to thank Sebastian Thöns, our supervisor at Lund University of Technology for his guidance, valuable discussions, and academic support during the course of this project.

We would like thank our friends and families for their support throughout the project and during the entire education.

Lund, 8th June 2026
Carl Larsson & Elias Jonasson

Notations and Symbols

Fatigue life parameters

N	Number of load cycles
N_C	Reference number of cycles
N_t	Total fatigue life
N_i	Fatigue crack initiation life
N_p	Fatigue crack propagation life

Stress and strain quantities

σ_{nom}	Nominal stress
σ_m	Membrane stress in the plate
σ_b	Bending stress in the plate
σ_s	Structural hot-spot stress, $\sigma_s = \sigma_m + \sigma_b$
σ_{HS}	Hot-spot stress
σ_{ENS}	Effective notch stress
σ_{nlp}	Non-linear stress peak
τ	Shear stress
ε_{hs}	Hot-spot strain

Stress cycle parameters

$\sigma_{s,\max}$	Maximum structural hot-spot stress in one load cycle
$\sigma_{s,\min}$	Minimum structural hot-spot stress in one load cycle
$\Delta\sigma$	Stress range, $\Delta\sigma = \sigma_{\max} - \sigma_{\min}$
$\Delta\sigma_s$	Structural hot-spot stress range
σ_{mean}	Mean stress, $\sigma_{\text{mean}} = \frac{\sigma_{\max}+\sigma_{\min}}{2}$
σ_{amp}	Stress amplitude, $\sigma_{\text{amp}} = \frac{\sigma_{\max}-\sigma_{\min}}{2}$
R	Stress ratio, $R = \frac{\sigma_{\min}}{\sigma_{\max}}$

Fatigue and fracture mechanics

$\Delta\sigma_C$	Reference fatigue strength at $N_C = 2 \times 10^6$ cycles
m	Slope of the S–N curve
ΔK_I	Stress intensity factor range
D_i	Fatigue damage per cycle (Miner's rule)

Material properties

E	Young's modulus
ν	Poisson's ratio

Finite element quantities

$\mathbf{K}$	Stiffness matrix
$\mathbf{f}$	Force vector
$\mathbf{a}$	Displacement vector

Contents

1 Introduction

1.1 Background

In the food processing industry, there is an increasing need to improve the durability and reliability of production equipment. Conveyor systems play a key role in freezing applications where stable operation over long periods is required to maintain product quality and safety.

JBT Marel is a global supplier of food processing equipment and offers the GYRoCOMPACT®freezer. This freezer uses a spiral conveyor belt to transport products through carefully controlled freezing environments. During operation, the conveyor belts are exposed to varying loads caused by belt tension, product weight, and stack load. Temperature variations also affect the conveyor system.

These complex loading scenarios influence the stress distribution and affect the fatigue behavior of critical components. Welded joints between rods and side links are often the most critical components of the conveyor belt. Fatigue failure in these welded connections can reduce the service life of the belt, leading to unplanned downtime and may compromise product quality.

For this reason, it is important to understand how different design choices influence the fatigue life of the conveyor belt. To support design decisions and ensure reliable performance, the fatigue life of the conveyor belt can be evaluated using both established theoretical and numerical methods. These analyses should be complemented by experimental testing to provide realistic data for model validation and to ensure that the conveyor system can meet both operational and lifetime requirements.

1.2 Aim and Objectives

The main objective of this thesis is to estimate the fatigue strength of both the NOVA conveyor belt and its enhanced version. Simplified fatigue tests provided by JBT Marel on both belts are used to validate and compare the theoretical models. To achieve the overall objective, the following sub-goals are defined.

- To identify and describe the dominant load systems acting on the conveyor belt, including belt tension, product load, and stack load.
- To analyse the stress distribution in critical components, with particular focus on welded joints between rods and side links.
- To estimate the fatigue life of the conveyor belt using established fatigue assessment methods.

- To compare theoretical fatigue life estimations with available experimental test data provided by JBT Marel.

Based on these objectives, the study aims to answer the following research questions.

- How does the introduction of a tension link affect the load distribution within the conveyor belt structure?
- To what extent do the numerical fatigue life estimations correlate with simplified fatigue tests performed for both conveyor belts?
- How does the weld throat thickness affect the fatigue life predictions?

1.3 Limitations

No experimental data were available for the vertical load systems. Therefore, reduction factors were only calculated for load systems with belt tension forces. The analyses still captured stress variations between the different methods, which mainly originated from the welding geometry.

Linear Elastic Fracture Mechanics could provide additional insight into crack propagation behaviour. However, this method requires detailed fracture models and fracture data that were not available within the scope of the project.

2 Theory

2.1 Fatigue

Fatigue is a type of damage that develops when a material is exposed to repeated loading. Even if the stress levels are low, fatigue failure can still occur after many load cycles [1]. The number of cycles to failure can vary significantly, from a few hundred to several million, and may occur without any noticeable plastic deformation. Repeated loading and unloading gradually reduces the strength of a structure or component over time. An example of fatigue damage is shown in Figure 2.1.

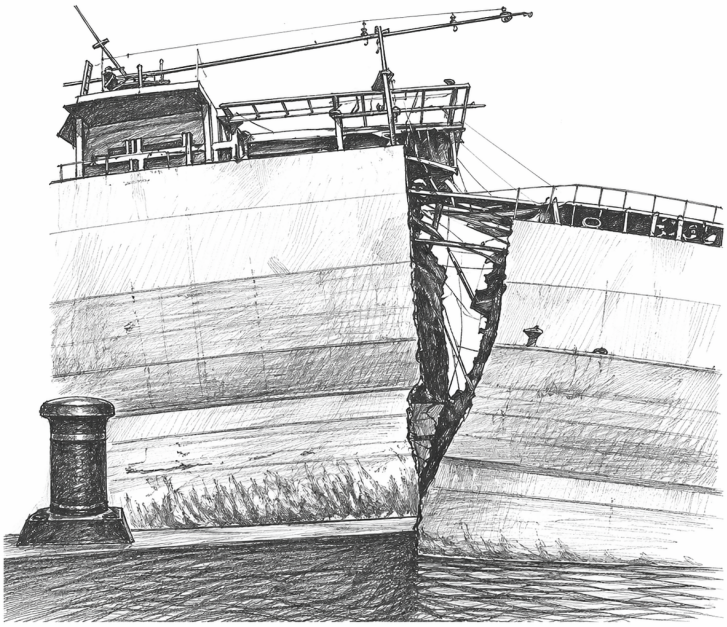

Figure 2.1: An example of severe fatigue damage in a ship hull caused by cyclic loading. Repeated stress variations can cause cracks to form and grow over time, which may eventually lead to structural failure [2].

Fatigue is not limited to metallic materials like steel. It can also occur in other engineering materials. For example, polymers and concrete can also experience fatigue damage. The way fatigue develops can vary between materials due to differences in their structure and mechanical properties [1].

2.1.1 Fatigue in Microstructure

Fatigue damage typically begins with small localised plastic deformations that cannot be recovered. When the load is repeated, these deformations can cause micro-cracks

to form, as shown in Figure 2.2. As the number of load cycles increases, the micro-cracks join together into a single dominant crack that propagates until fatigue failure occurs [3].

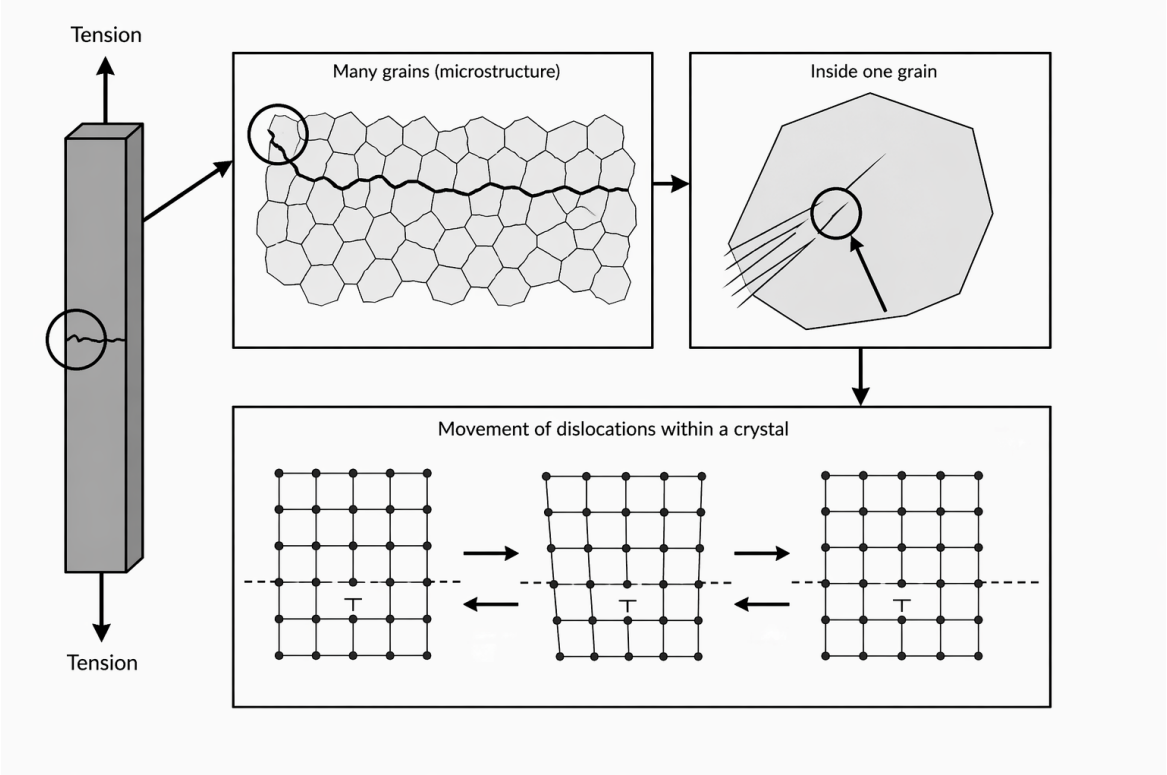

Figure 2.2: Illustration showing how a crack occurs between grains when a load is applied to a structure. The figure shows how a crack develop between material grains and how dislocation movement within the crystal contributes to fatigue damage and crack growth [3].

The fatigue life N_t can be divided into two main parts, the fatigue crack initiation life N_i and the fatigue crack propagation life N_p. These two stages differ because crack initiation depends on the material and its properties, whereas crack propagation is less independent of them. In some cases, most of the fatigue life is consumed before a crack forms. In other cases, cracks can appear early if defects are already present in the structure or component [4].

A crack nucleus is the formation of the first very small crack. This typically occurs early in the fatigue process when repeated loading begins, provided that the stress level exceeds the fatigue limit. Cracks often arise due to small internal movements in the material, known as slip bands. These are localised permanent shear deformations in the crystalline structure caused by movement within the material, as shown in Figure 2.3. The formation of slip bands can occupy a large part of the fatigue life. Initially, the crack grows slowly and irregularly. Later, the growth becomes more stable and continues in a more defined direction. Crack propagation begins when the crack growth becomes stable and directional [4].

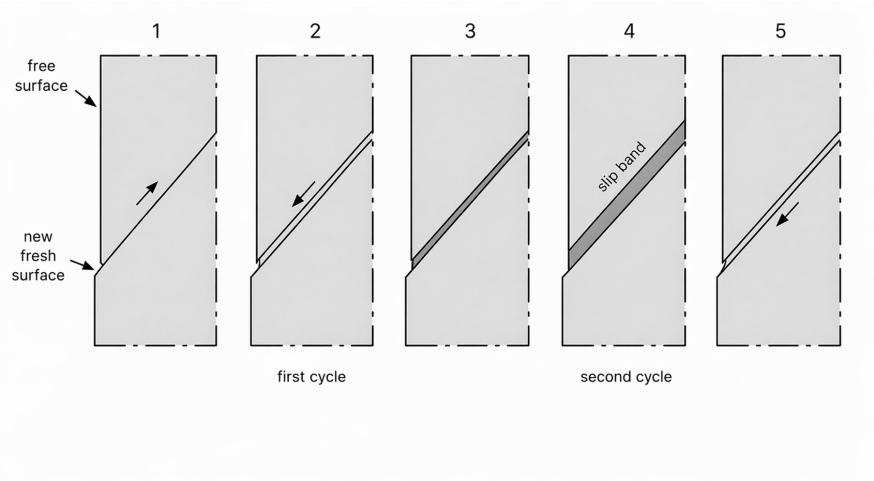

Figure 2.3: Illustration of slip bands from a shear driven process in the material microstructure during cyclic loading [3].

As micro-cracks grow across several grains, they change the local stress field and increase the stress concentration at the crack tip. Continued cyclic loading causes the micro-cracks to join together into a dominant crack. Over time, the crack growth direction gradually aligns perpendicular to the maximum principal stress. During propagation, crack growth remains influenced by the crystal structure and typically follows a zigzag pattern. In metals, fatigue cracks generally grow through the grains rather than along the grain boundaries [3].

Fatigue fracture surfaces reveal characteristic features that distinguish them from static failures. Near the crack origin, the surface is typically very smooth due to repeated rubbing of the crack faces during slow propagation. At the microscopic level, small lines called striations may be observed. These lines represent how a crack progresses per load cycle. At the macroscopic scale parallel growth bands, also known as beach marks may appear and provide information about crack origin and variations in loading conditions [3].

2.1.2 Fatigue in Welds

According to Radaj [5], fatigue performance is a critical aspect in the design of welded structures subjected to cyclic loading. In high tensile steels, welded joints often determine the overall fatigue strength due to the stress concentrations and local material variations introduced during the welding process. High strength steels, such as case-hardened and fine-grained structural steels, are commonly used to reduce structural weight and material consumption. Although these materials generally have higher endurance limits in smooth and unnotched specimens, this advantage becomes smaller in welded joints where notch effects strongly influence the fatigue behaviour. As a result, welded or notched components made from both low- and high-strength steels often show similar fatigue lives. The benefits of using high tensile steels are most significant when notch effects are minimised and the mean stress level is sufficiently high.

Geometric Discontinuities

Although geometrical stress concentrations are not the only factors affecting the fatigue strength of welded structures, they play a significant role in fatigue crack initiation. Typical geometric discontinuities in welded joints include abrupt changes in cross-section, weld reinforcement, sharp weld toes and weld roots as shown in Figure 2.4 [3].

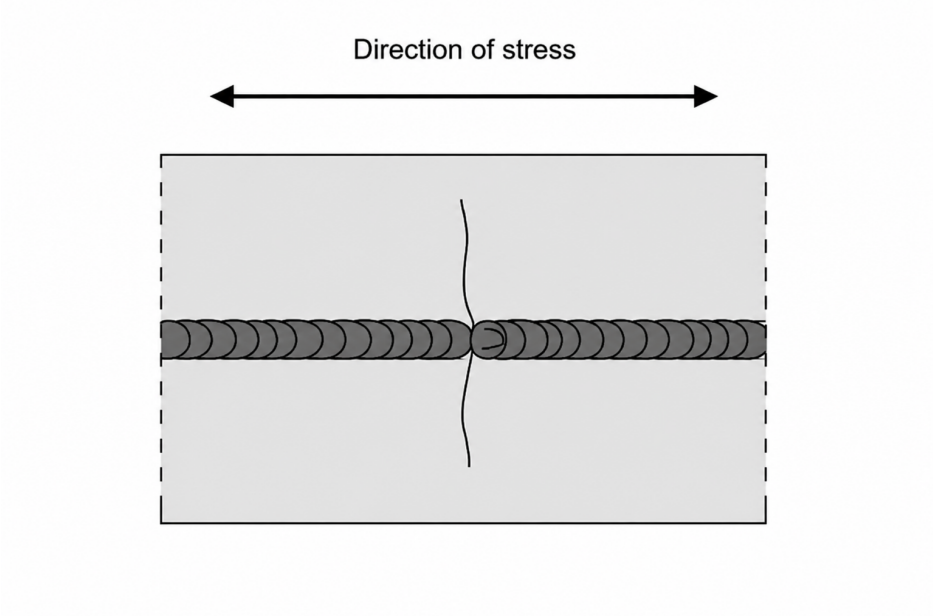

Figure 2.4: Example of a weld discontinuity causing local stress concentrations that may contribute to fatigue crack initiation [3].

These features affect the stress distribution and locally amplify the stresses, which can create regions where fatigue cracks can initiate. In particular, the weld toe represents a critical geometric notch where fatigue cracks frequently originate. This may especially occur when the applied load is perpendicular to the weld direction [6].

Geometric discontinuities can be reduced through improved detailing. For example by using smoother weld profiles and more favourable joint geometries. Since the geometric design is largely controllable, careful detailing is one of the most effective ways to improve fatigue resistance [7].

Material Defects and Weld Imperfections

In addition to geometric effects, the welding process introduces material defects. These defects can consist of microstructural discontinuities that act as local stress raisers and crack initiation zones. Although these imperfections are typically small, they can behave as crack-like defects from which fatigue cracks can grow under cyclic loading. Common weld defects include undercuts, porosity, inclusions, incomplete penetration, root defects and lack of fusion [7].

An undercut at the weld toe is one of the most common weld imperfections and is present to varying degrees in most welded joints. When the load is applied perpen-

dicular to the weld line undercuts can significantly reduce the fatigue strength due to their sharp notch-like geometry. Similar crack-like defects may also occur at the weld root in butt welds [8]. An example of an undercut weld and the associated stress distribution is shown in Figure 2.5.

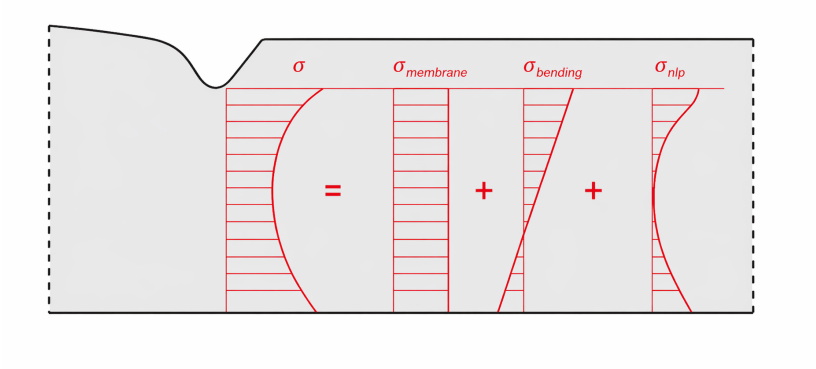

Figure 2.5: Illustration of a undercut weld and the stress distribution through a steel plate. The total stress distribution consist of membrane stress, bending stress and nonlinear stress [9].

Another common weld defect is porosity, which occurs when gas becomes trapped in the weld during cooling. These pores can act as initiation points for fatigue cracks, as shown in Figure 2.6. Inclusions can form when slag is not properly removed between weld passes. Root defects and incomplete penetration may arise from improper joint preparation or unsuitable welding parameters which may result in internal defects in the weld. Lack of fusion can happen when the heat is too low or when the welding is done too fast. This prevents proper bonding between the weld metal and the base material and is particularly harmful under cyclic loading [3].

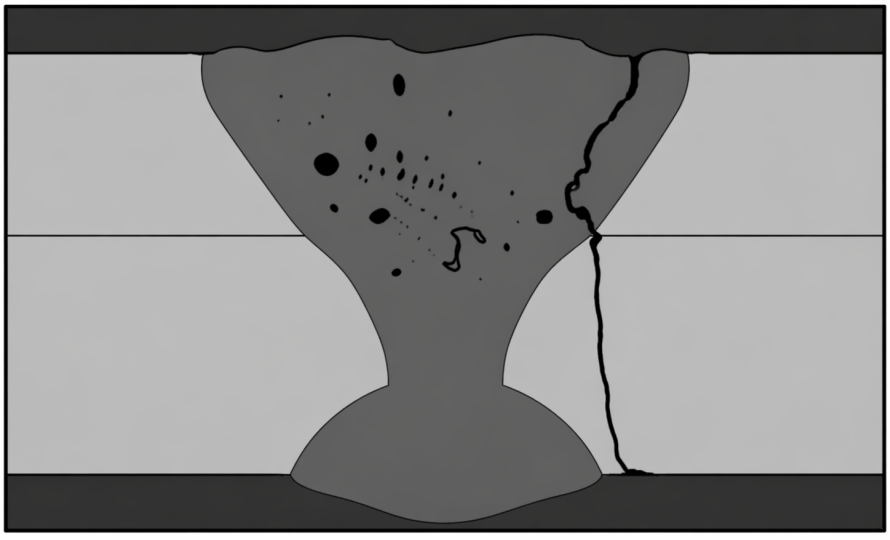

Figure 2.6: Illustration of porosity defects in a butt weld and how these defects may initiate fatigue cracks in both the weld and the base plate [10].

It is not practical to include all weld defects in fatigue analyses. Instead, their com-

bined effects are taken into account through experimental fatigue testing and included in fatigue strength classifications used in structural design standards. Weld defects cannot be completely eliminated, but their impact can be reduced through proper welding procedures and quality control [11].

Residual Stresses

According to Schijve [12], residual stresses in welds are caused by temperature changes during the welding process. When the weld cools down, it tries to shrink, but the surrounding base material prevents this from happening. This often leads to the development of tensile residual stresses along the weld direction. If the welded joint is later subjected to loading in the same direction, these stresses may increase the risk of fatigue crack initiation, especially in regions where surface imperfections exist.

In addition to longitudinal stresses, welding can also introduce residual stresses across the weld. These stresses are usually tensile at the surface and compressive within the material, as shown in Figure 2.7.

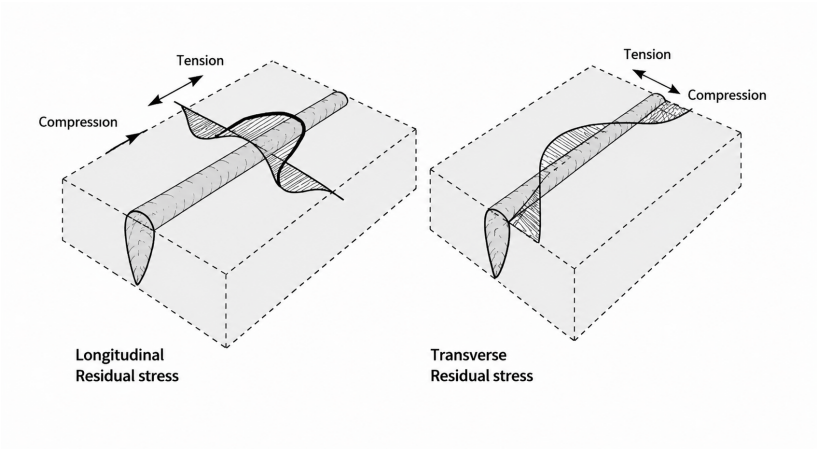

Figure 2.7: Illustration of residual stresses in longitudinal and transverse direction generated during welding and the associated stress fields [13].

2.2 Fatigue Terms and Explanation of Definitions

Steel structures are often exposed to fatigue loading that changes during their service life. In real structures the loads change over time [3]. In laboratory testing, a common method is to use constant-amplitude loading, where the material is repeatedly loaded between a maximum and a minimum stress level. The difference between the highest and lowest stress level is called the stress range and is given by $\Delta\sigma = \sigma_{\max} - \sigma_{\min}$.

The mean stress is given by $\sigma_{\text{mean}} = \frac{\sigma_{\max}+\sigma_{\min}}{2}$, and the stress amplitude is given by $\sigma_{\text{amp}} = \frac{\sigma_{\max}-\sigma_{\min}}{2}$ [11]. Figure 2.8 illustrates the different parameters associated with constant-amplitude loading.

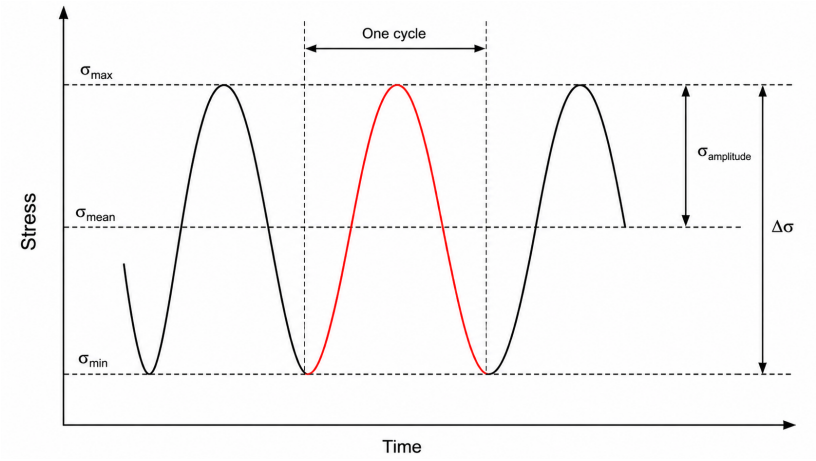

Figure 2.8: Illustration of how the stress varies over time during a constant amplitude loading, including minimum, maximum, amplitude and stress range [14].

The stress ratio R describes how the minimum stress relates to the maximum stress and is defined as $R = \frac{\sigma_{\min}}{\sigma_{\max}}$ [3]. Figure 2.9 shows how different values of the stress ratio correspond to different loading conditions.

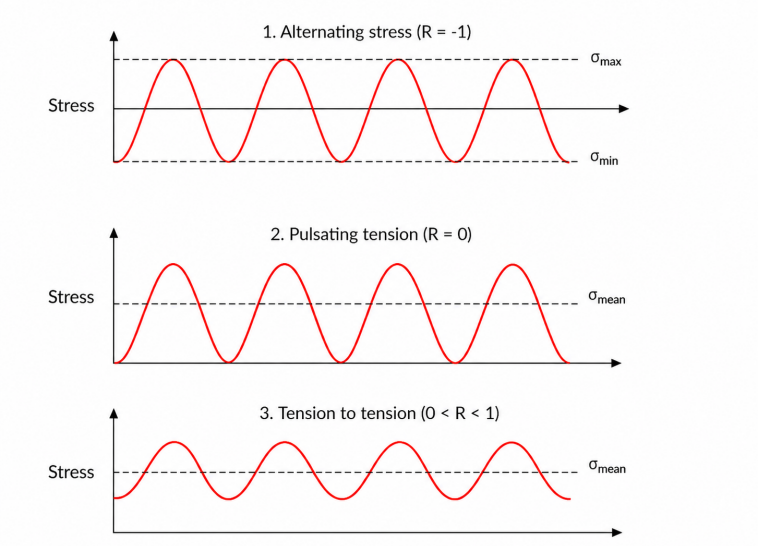

Figure 2.9: Illustration of different stress ratios showing how the minimum and maximum stress levels vary over time during cyclic loading [13].

As shown in Figure 2.9, $R = -1$ means that the stress varies between tension and compression [3], while $0 \leq R \leq 1$ means that the stress remains in tension.

2.3 S–N Curves

The number of cycles that a component can withstand depends mainly on the stress range [3]. When analysing fatigue, the main purpose is to estimate how many load cycles a component can endure under different stress levels. Fatigue behaviour is often described using S–N curves, also called Wöhler diagrams. S–N curves describe the relationship between the stress level and the number of cycles the material can withstand before failure, and they are often presented on a log–log scale.

Once fatigue experiments have been performed on a steel component, the resulting test data are used to create these S-N curves [3]. Figure 2.10 shows an example of an S-N curve.

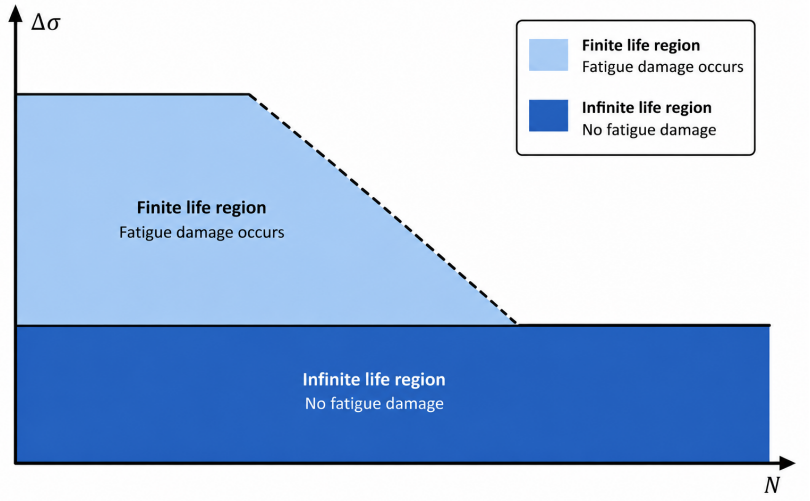

Figure 2.10: Illustration of a S-N curve used in fatigue analysis, showing the relationship between the stress range and the number of load cycles to failure. The finite region represent stress levels where fatigue failure occurs after a certain number of load cycles. The infinite life region corresponds to stress levels below the fatigue limit [13].

The upper left part of the curve represents high stress levels. In this region, plastic deformation occurs quickly, often resulting in failure after only a few load cycles. This is referred to as low-cycle fatigue. The lower right region represents low stress levels in the steel component. Under these conditions, the material can withstand a very large number of cycles without failure [3].

Fatigue crack growth behaviour is commonly described using experimental data for a given material. In experiments, a cracked specimen is subjected to cyclic loading with a constant stress range defined as $\Delta\sigma = \sigma_{\max} - \sigma_{\min}$. Crack growth behaviour is typically described using relationships between crack length, load cycles, and stress intensity factors. The stress intensity factor range is given by $\Delta K_I = K_{I\,\max} - K_{I\,\min}$. Where $K_{I\,\max}$ represent the maximum stress in one cycle and the $K_{I\,\min}$ represent the minimum stress in one cycle. The stress intensity factors also depends on the crack size and an geometry factor [15].

The crack growth rate is expressed as $\frac{da}{dN}$, which describes how fast the crack length increases per load cycle [15]. Experimental studies presented by Paris in 1962 [3] show that, for a given load ratio, the relationship between crack growth rate and the stress intensity factor can be represented by a single curve for a specific material. The crack growth curve is typically divided into three regions, often referred to as A, B, and C [15].

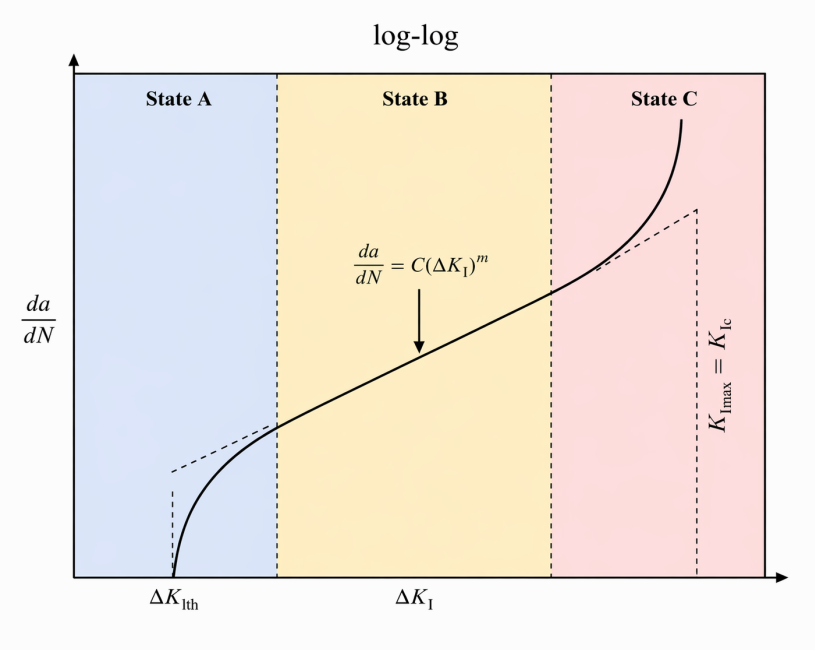

Figure 2.11: Fatigue crack growth curve showing the relationship between crack growth and the stress intensity factor range during different stages of the crack propagation [15] .

- State A: In this part of the curve, the crack grows very slowly and propagation occurs below the fatigue threshold. $\Delta K_{I,\text{th}}$. This threshold represents the stress intensity factor range below which crack propagation is very limited or does not occur [15].
- State B: In this region, the crack growth follows the relation $da/dN = C(\Delta K_I)^m$ where C and m are material constants determined from experimental tests. In this part of the curve the slope is constant, which means that the crack grows in a stable and predictable manner [15].
- State C: In this part, very high stress levels occur and the crack grows rapidly as $K_{I,\text{max}}$ gets close to the fracture toughness K_{Ic}. The fracture toughness represents the critical stress intensity factor of the material. As a result, this stage represents only a small portion of the total fatigue life and is of minor importance in fatigue analysis [15].

2.3.1 Rainflow

When a steel structure is exposed to variable-amplitude loading, the stress varies over time and creates a complex stress history that includes peaks and valleys. To perform fatigue analysis using S-N curves, this stress history must be converted into a set of stress cycles with corresponding stress ranges [16]. The rainflow counting method is commonly used for this purpose. The method transforms the irregular stress history into a series of closed stress cycles. Each cycle is defined by a stress range and a mean stress. These cycles can then be analysed in the same way as constant-amplitude loading used in laboratory fatigue tests. The method identifies the load cycles that contribute to fatigue damage by pairing stress reversal points in a way that reflects the material response to repeated loading over time. By doing this, the relevant stress cycles contributing to fatigue damage are extracted from the loading history and used in the analysis. An illustration of the rainflow method can be seen in Figure 2.12.

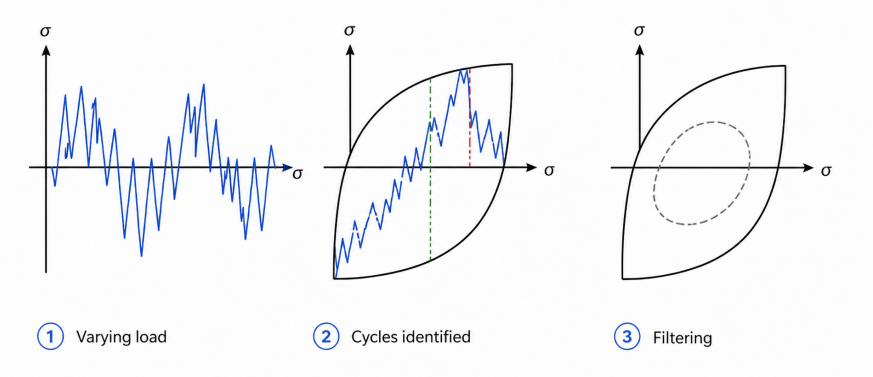

Figure 2.12: Illustration of the rainflow method, including varying load histories, cycle identification and cycle filtering used in fatigue analysis [16].

2.3.2 Palmgren–Miner Rule

The Palmgren–Miner rule assumes that fatigue damage accumulates linearly [17]. Each stress cycle therefore contributes a fraction of damage based on its stress amplitude. The damage for each stress level is calculated according to Equation 2.1.

$$D_i = \frac{n_i}{N_i} \tag{2.1}$$

The total accumulated damage is calculated using Equation 2.2.

$$D = \sum_{i=1}^{k} \frac{n_i}{N_i} \tag{2.2}$$

Where N_i is the number of cycles to failure at the stress level corresponding to n_i, and k is the total number of stress levels.

2.4 Fatigue Life Assessment Approaches

2.4.1 Nominal Stress Method

The nominal stress method considers the combined stresses resulting from bending moments and normal forces in a structural detail, as illustrated in Figure 2.13 [3].

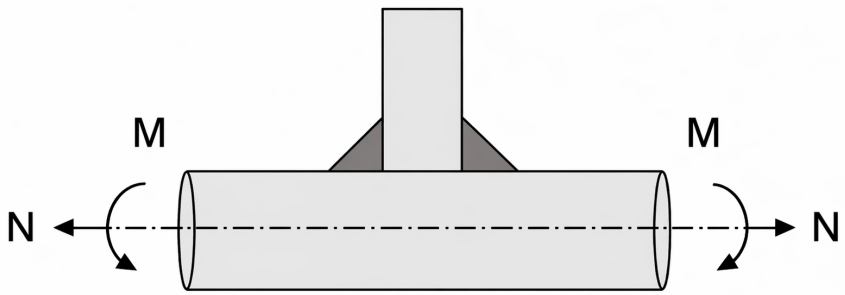

Figure 2.13: Illustrating the nominal stress acting in the welded joint, representing the global stress distribution acting in the welded joint [13].

The nominal stress method is based on the use of an appropriate S–N curve for the structure. The nominal stress is calculated at the critical location, and the fatigue life is estimated by combining the S–N curve with a fatigue damage accumulation rule. In this method, the stress is determined using simplified stress calculations based on the applied loads and the cross-sectional geometry. Local stress concentrations caused by the weld geometry are not directly included in the analysis [18].

S–N curves are generally derived from fatigue tests on smooth samples under controlled laboratory conditions. Because of this, these curves do not account for factors such as stress concentrations, size effects, surface roughness, and residual stresses, which may influence the fatigue behaviour of real components. In practical reality, the S–N curve therefore needs to be modified to include these effects. This is commonly done by introducing modification factors, including stress concentration factors, size factors, and surface factors. By applying these factors, the nominal stress method can provide a more realistic evaluation of the fatigue life [18].

Finite Element Analysis According to Nominal Stress

When using the nominal stress method, it is often not necessary to use the finite element models. If the loads, geometry, and boundary conditions are known, simple analytical calculations are sufficient.

If the finite element method is applied, a relatively simple and rough mesh may be used. However, care must be taken to ensure that stress concentration effects associ-

ated with the local geometry of the welded joint are excluded when determining the modified nominal stress. For fillet weld analyses using coarse finite element meshes, nominal stresses should be evaluated based on nodal forces extracted from a cross-section through the weld. This approach is preferred over using element stresses in order to avoid underestimation of stress levels [19].

2.4.2 Hot Spot Stress Method

The hot spot stress method for welded joints is used when the principal stress acts mainly transverse to the weld toe or when fatigue crack initiation is expected to start at this location. In a welded joint, the weld toe introduces a geometric discontinuity. This leads to a non-linear stress distribution through the thickness. The stress state can be described using three components. The membrane stress, bending stress and a local peak stress [19]. An illustration of this is shown in Figure 2.14.

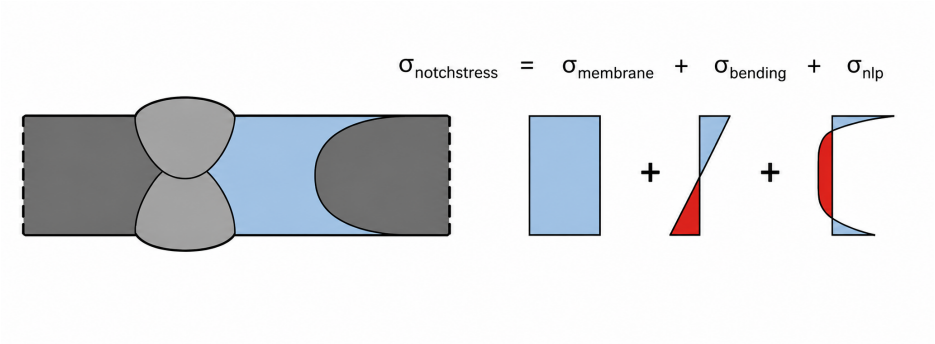

Figure 2.14: Illustration showing the stress distribution through a welded joint. The total stress distribution consists of the membrane, bending and nonlinear stress and are used in the hot spot method [19].

The stress components can be obtained by decomposing the stress distribution, $\sigma(x)$ through the thickness, where x varies from (0) at one surface to (t) at the opposite surface. The membrane stress (σ_{membrane}) has the same stress value across the thickness. The shell bending stress (σ_{bending}) changes linearly through the thickness. The non-linear stress peak (σ_{nlp}) is self-equilibrating and depends on the size of the weld as well as the weld toe geometry. All three stress components can be calculated using the following equations [20].

$$\sigma_{\text{membrane}} = \frac{1}{t}\int_{x=0}^{x=t} \sigma(x)\,\mathrm{d}x \tag{2.3}$$

$$\sigma_{\text{bending}} = \frac{\sigma}{t^2}\int_{x=0}^{x=t} (\sigma(x) - \sigma_{membrane})\left(\frac{t}{2} - x\right)\mathrm{d}x \tag{2.4}$$

$$\sigma_{\text{nlp}}(x) = \sigma(x) - \sigma_{\text{membrane}} - \sigma_{\text{bending}}\left(1 - \frac{2x}{t}\right) \tag{2.5}$$

The local notch effect is usually not evaluated directly. Instead, its effect is included in the corresponding S–N curves [20]. This is because the exact weld geometry is not known during the design phase. The structural hot spot stress is therefore defined by summing only the two linear stress components according to the following equation:

$$\sigma_{\text{hotspot}} = \sigma_{\text{membrane}} + \sigma_{\text{bending}} \tag{2.6}$$

Where σ_{hotspot} is the structural hot-spot stress.

The hot spot stress is determined by evaluating stresses at selected reference points, as shown in Figure 2.15. The method is mainly used for assessing the weld toe. Some examples are shown in Figure 2.19. However, it can also be extended to other potential fatigue crack initiation locations. This can be done by using the structural hot-spot stress on the surface of interest as an indication of the stress state. The S-N curves or stress concentration factors used for verification depend largely on the geometric and dimensional parameters and are only valid within the range of these parameters [20].

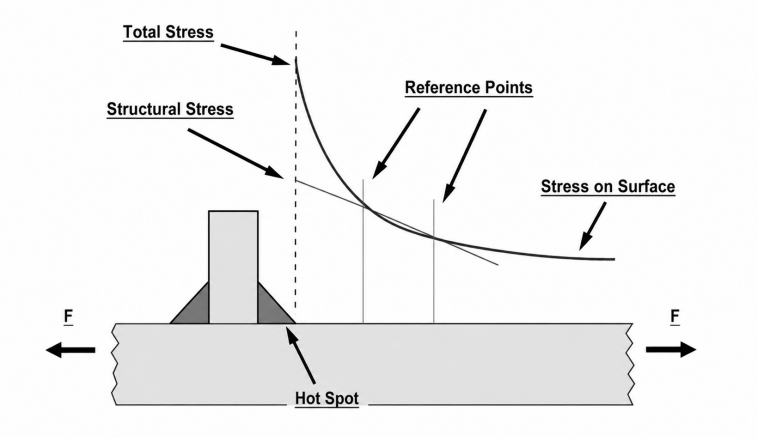

Figure 2.15: Hot spot stress definition and the illustration of the reference points used for extrapolation in calculations of the hot spot stress. The figure also shows how the stress gradient increases closer to the weld toe along the thick line [21].

According to the IIW recommendations and the Designers Guide to the structural hot spot approach, two types of hot spots in welded details can be identified. Type "a" corresponds to a weld toe located on a plate surface. Type "b" corresponds to a weld toe located at a plate edge. These two configurations are illustrated in Figure 2.16 [19].

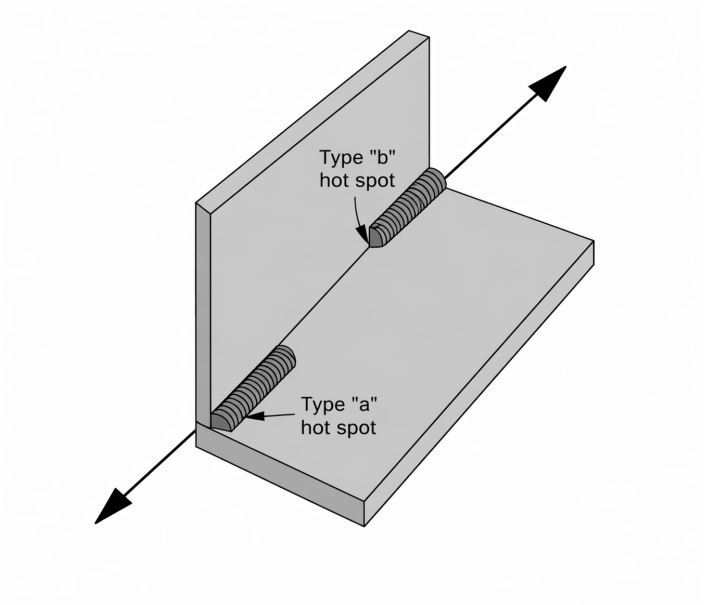

Figure 2.16: Type ”a” and type ”b” hot spot weld configurations used for fatigue evaluation in the hot spot method [20].

Type ”a” Hot Spot

Figure 2.17 illustrates how the stress distribution through the plate thickness changes near a type ”a” hot spot. At a distance of $0.4t$ from the weld toe, the local stress peak becomes significantly smaller, and the stress distribution is close to linear. This behaviour is used in the extrapolation procedure for estimating the structural hot-spot stress.

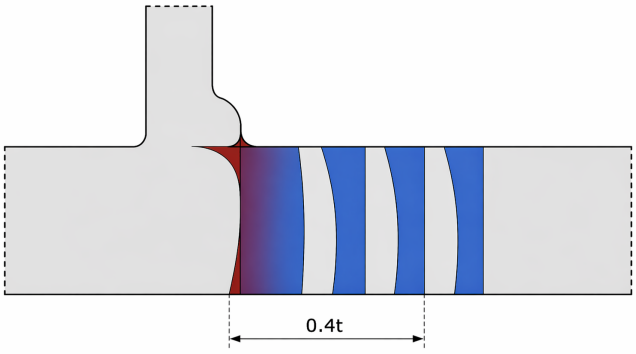

Figure 2.17: Stress distribution through a plate, where the red region represents non-linear stress and blue linear stress for a type ”a” hot spot weld in the toe [19].

Type ”a” Hot Spot Using Strain Gauges

During fatigue testing, this structural stress can be determined using strain gauges and extrapolation. Two strain gauges labeled A and B, are placed at fixed distances from

the weld toe as seen in Figure 2.18. Based on these measurements, the structural strain at the hot-spot location is determined by linear extrapolation. The structural hot spot method assumes that the stress field outside the local region varies approximately linearly through the chosen reference points, as seen in Figure 2.15.

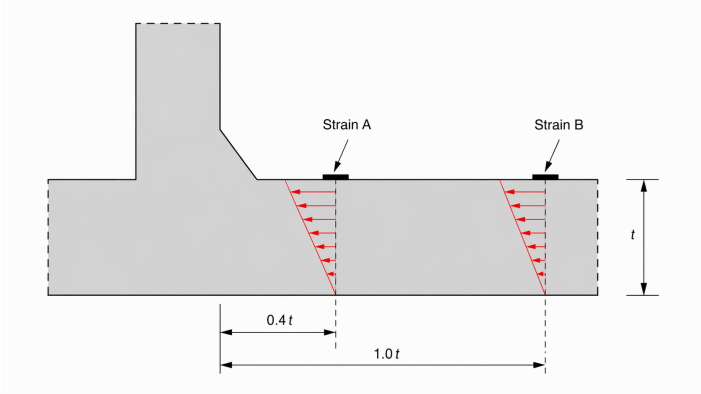

Figure 2.18: Gauges are placed at locations "A" and "B" used for the hot spot strain evaluation near the weld [20].

The structural hot-spot strain is then calculated according to the following equation after extrapolation is perfomed:

$$\varepsilon_{\text{hotspot}} = 1.67\,\varepsilon_A - 0.67\,\varepsilon_B \tag{2.7}$$

Where ε_A and ε_B are the strains measured at distances $0.4t$ and $1.0t$ from the weld toe.

There are cases where linear extrapolation may lead to an underestimation of the structural hot-spot stress [19]. This may occur when a loaded plate rests on a relatively stiff elastic foundation or in stiff structural configurations where the stress field is influenced by surrounding components. In such situations the stress increases in a non-linear manner as the weld toe is approached. In these cases it is more appropriate to apply a quadratic extrapolation method using reference points located at distances of $0.4t$, $0.9t$, and $1.4t$ from the weld toe. The structural hot-spot strain is then given by the following equation below.

$$\varepsilon_{\text{hotspot}} = 2.52\,\varepsilon_A - 2.24\,\varepsilon_B + 0.72\,\varepsilon_C \tag{2.8}$$

After the strain values have been extracted at the reference points, the structural hot-spot stress can be calculated. This approach is valid only for a uniaxial stress state [20]. A uniaxial stress state means that one stress component dominates and the other stress components are small enough to be neglected. The relationship is given by the following equation.

$$\sigma_{\text{hotspot}} = E\,\varepsilon_{\text{hotspot}} \tag{2.9}$$

Where E is the elastic modulus and ε_{hs} is the structural hot-spot strain.

Type "b" Hot Spot

Hot spot type "b" differs from type "a" because for type "b" details the stress field is mainly governed by the plate edge geometry rather than the local weld profile [19]. Therefore, IIW recommends fixed reference points. These reference points are placed at the distances 4, 8, and 12 mm. The measured strains are then converted into stresses and the structural hot-spot stress is calculated using equation 2.10 [19].

$$\sigma_{\text{hotspot}} = 3\,\sigma_{4\,\text{mm}} - 3\,\sigma_{8\,\text{mm}} + \sigma_{12\,\text{mm}} \tag{2.10}$$

2.4.3 Classification of Welded Joints Using the Hot Spot Method

In the hot-spot stress method, welded joints can be divided into different categories depending on how the load is transferred through the weld [19]. These categories include load-carrying, partially load-carrying, and non-load-carrying welds. Figure 2.19 illustrates examples of these different weld categories.

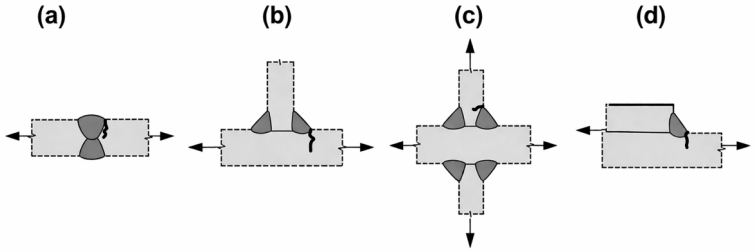

Figure 2.19: Welds shown in cases (a) and (c) are fully load-carrying. In case (b), the weld does not primarily carry the applied load. Welds at cover plates or collar plates, as shown in (d), carry part of the load and are therefore classified as partially load-carrying [19].

If there is any uncertainty regarding the classification of a weld, it should be assumed to be load-carrying.

Finite Element Analysis According to Hot Spot

When modeling hot-spot stresses using finite element analysis, the goal is to determine the structural stress at the weld toe or weld end, since fatigue cracks may initiate at these locations. The first step is to identify where critical hot-spot points are most likely to occur. This is done by choosing between the two previously defined hot-spot types, Type "a" and Type "b" [20].

Finite element analysis is performed under linear-elastic conditions, since plastic deformation is not expected under fatigue design loads [22]. Shell or plate elements

may be used for modelling thin plate structures because these elements can represent both membrane and bending stresses in the plate. For more complex geometries, solid elements may also be used [20].

To capture the the stresses near the hot spot, a sufficiently refined mesh is required. The element size is generally chosen within the range of $t/4$ to $t/10$, where t denotes the plate thickness [19]. This makes it possible to evaluate the structural hot-spot stress. The detailed weld geometry is not included in the model since it is not considered in the hot-spot method.

2.4.4 Effective Notch Stress Method

Fatigue failure is, as mentioned earlier, a common problem in welded steel structures, especially at locations where geometric discontinuities exist. Features such as holes, welds, or sudden changes in geometry create stress concentrations that strongly influence the fatigue strength. These localised stresses are referred to as notch stresses and are important when predicting fatigue crack initiation.

The effective notch stress method considers the local stress concentrations at either the weld toe or the weld root. The approach was originally introduced by Heinrich Neuber and is based on linear-elastic theory [13].

In this method, a fictitious notch radius is introduced to reduce the stress concentrations that appear at sharp notches. The concept is illustrated in Figure 2.20.

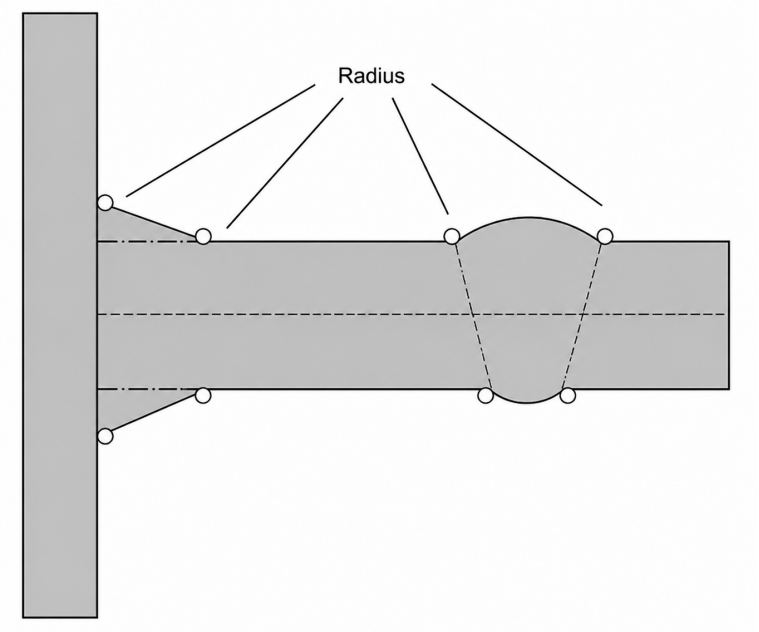

Figure 2.20: Illustration of fictitious notch radius used in effective notch method to reduce the influence of sharp geometric in welded joints [20].

The choice of the S-N curve to calculate the effective notch stress depends on the notch radius being used. The S-N curves for the effective notch method were established using fatigue test data obtained from welded specimens [11]. According to IIW [11],

the following characteristic fatigue strengths should be used for different notch radii. The fatigue strengths are summarized in Table 2.1.

Table 2.1: Fatigue strength classes for steel welds used in the effective notch stress method and implemented in the finite element analyses [11].

Notch radii [mm]	Characteristic fatigue strength
1	FAT 225
0,05	FAT 630

From the characteristic fatigue strength, an S–N curve can be derived. Figure 2.21 shows the S–N curves corresponding to different FAT classes.

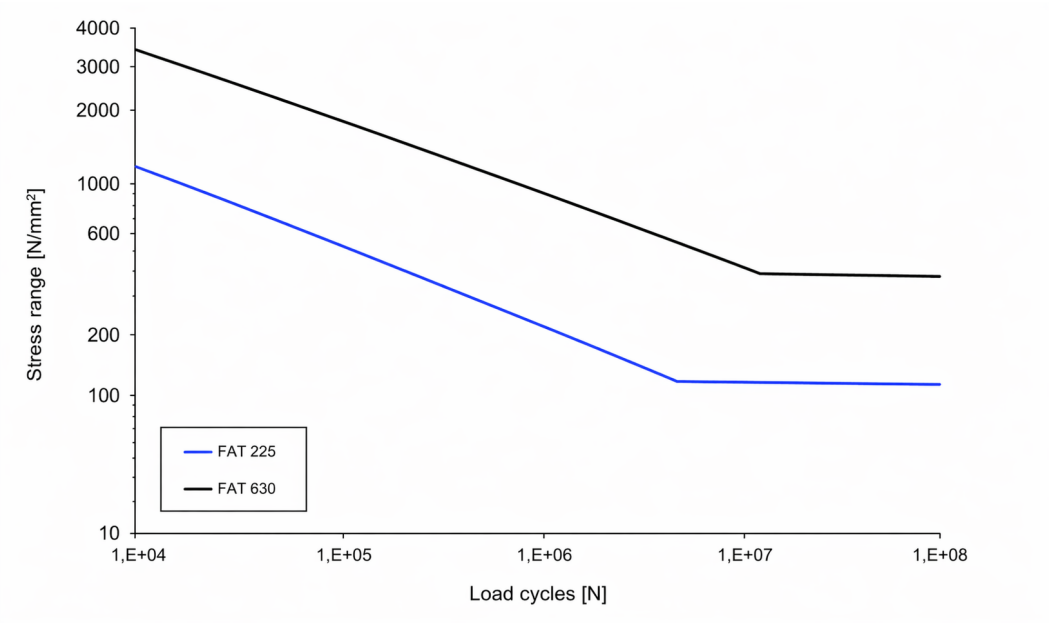

Figure 2.21: S-N curves used for different FAT-classes in fatigue evaluation of welded structures. The blue line represent Fat 225 while the black line represent fat 630, both are for the von Mises stresses [13].

Finite Element Analysis According to Effective Notch Stress Method

As mentioned previously, one of the challenges when performing stress calculations using the finite element method is that very high stress concentrations may occur at the weld toe or weld root [11]. In numerical models, this can lead to stress values that approach infinity and therefore become unsuitable for fatigue assessment.

To address this issue, the recommendations provided by IIW [11] suggest introducing a fictitious notch radius of 1 mm for steel structures with plate thicknesses greater than 5 mm. For plates with a thicknesses smaller than 5 mm, a fictitious radius of 0.05 mm may be used. This radius replaces the irregular weld geometry present in real welded joints. The radius can be introduced either at the weld toe or at the weld root. Figure 2.22 illustrates how the effective notch radius is implemented in the finite element model.

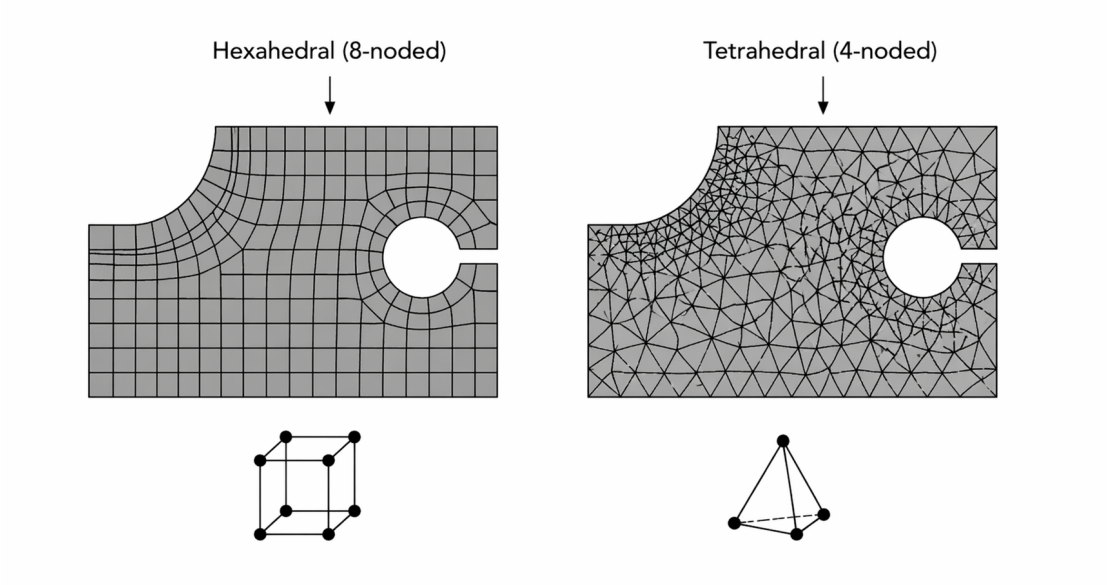

Figure 2.22: Illustration showing how the radius and refined mesh is implemented into the finite element model accuretly to capture stress variations in the weld [22].

When implementing the radius into the finite element model a keyhole or U shaped geometry is often used, as seen in Figure 2.23. The keyhole geometry is constructed so that the vertex of the reference circle is located at the weld root while the length of the non-welded root faces is maintained. This preserves the essential geometric characteristics of the real joint while still introducing the reference radius required by the method. In this way, the local stress distribution at the weld root can be represented without altering the overall joint configuration [11].

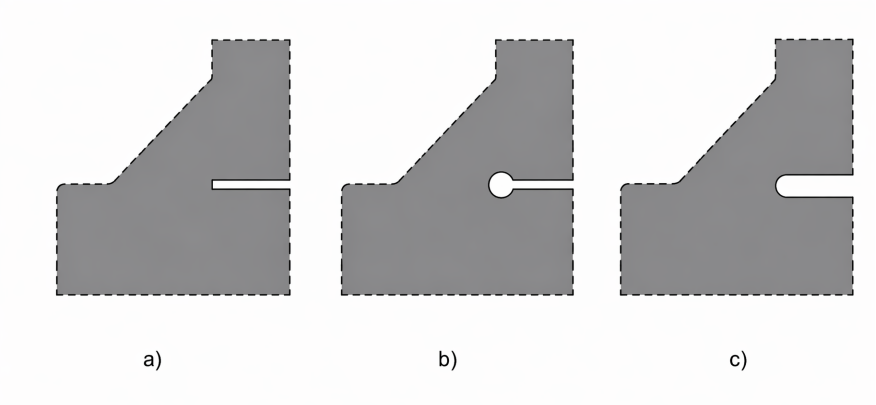

Figure 2.23: Illustration of the different notch geometries when using the effective notch and implemented in the finite element models, including the original sharp notch, keyhole notch, U-shaped notch [11].

When applying the effective notch stress method, a conservative meshing strategy is required. The weld and surrounding regions must be finely meshed since the fatigue stress is evaluated directly at the notch. A refined mesh ensures that the stresses converge to realistic values instead of increasing towards infinity at sharp geometric discontinuities.

The size of the element could be chosen according to Table 2.2. An example of how the mesh is applied is shown in Figure 2.22.

Table 2.2: IIW recommendations for fictitious notch radii and corresponding mesh sizes used in effective notch stress analysis [11].

Element formulation	**Relative mesh size**	$r = 1$ **mm** ($t \geq 5$ **mm**)	$r = 0.05$ **mm** ($t < 5$ **mm**)
Hexahedral, quadratic	$\leq r/4$	0.25 mm	0.012 mm
Hexahedral, linear	$\leq r/6$	0.15 mm	0.008 mm
Tetrahedral, quadratic	$\leq r/6$	0.15 mm	0.008 mm

2.5 Fatigue Behavior of Spot Welds

Although extensive research exists on the fatigue life of resistance spot welds, understanding fatigue crack initiation and propagation remains challenging. This is primarily because cracks originate at the sheet interface, which is a critical region with complex micro-structural changes, making fracture mechanics analysis difficult. Additionally, cracks are not easily observable until significant damage has occurred, which requires the use of indirect measurement techniques [23].

Crack initiation is strongly influenced by stress concentrations, particularly around the spot weld circumference. Studies show that cracks may initiate close to the spot edge and can occur early in the fatigue life, sometimes after as little as 10% of the total fatigue life has elapsed. However, visible crack growth is often not observed until approximately 50% of the total fatigue life has been reached. Experimental observations also indicate that the stiffness remains largely unaffected until the cracks reach a considerable size [23].

For spot welds, there are three different failure methods. Either pull out failure, plug failure or interfacial failure, which could be seen in Figure 2.24.

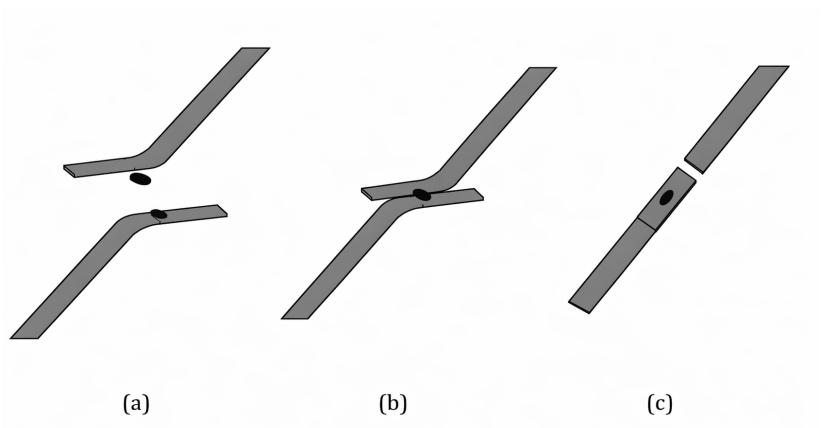

Figure 2.24: Three different failure modes for spot welds during cyclic loading. a) Pull out failure b) Plug failure c) Interfacial failure [23].

A study by Ibrahim T. et al. [24] investigate how fatigue behavior is affected by the tensile shear of spot welds, in particular, focusing on the influence of geometric parameters and loading conditions on fatigue life. Experimental tests were conducted on tensile shear specimens, subjected to cyclic loading, where different failure modes were observed depending on the applied load levels. At higher loads, fatigue failure occurred primarily through shear fracture in the weld nugget, whereas at lower loads, crack initiation and propagation were observed in the surrounding base material. These findings demonstrate that the fatigue behavior of spot-welded joints is highly dependent on load magnitude and stress distribution.

The study [24] also highlights the critical role of geometric parameters in fatigue performance. Factors such as sheet thickness, weld nugget diameter and plate width significantly influence stress distribution and crack initiation. Increased sheet thickness and weld size generally increase fatigue resistance by reducing stress concentrations, while inappropriate geometric configurations can accelerate crack growth. Furthermore, residual stresses generated during welding are shown to play a crucial role in fatigue behavior, where tensile residual stresses promote crack initiation and reduce fatigue life, while compressive residual stresses can delay crack propagation.

2.6 Bilinear Isotropic Hardening

Bilinear isotropic hardening is a simple elasto-plastic material model that describes the mechanical response of metals after yielding [25]. The theory behind it assumes that the material behaves linear elastic until it reaches the yield stress, after which plastic deformation occurs, and the yield surface expands in all directions.

When the stress reaches the initial yield strength, plastic deformation begins. After this stage, bilinear isotropic hardening is used to approximate the plastic region. The following relation is used to describe the isotropic hardening, as shown in Equation 2.11 [25].

$$\sigma(h) = YS + E_t(\varepsilon^p) \tag{2.11}$$

YS describes the initial yield strength, E_t is the tangent modulus and ε^p is the accumulated plastic strain.

3 Method

3.1 Method–selection Rationale

In the thesis, three methods have been used to evaluate the fatigue life of the welds; the effective notch-, hot spot- and nominal stress methods. These three methods were used to capture both the local and global stress and fatigue behavior of the conveyor belt. This was necessary because the research questions involve both load redistribution and local weld fatigue behavior. Therefore, all three methods were necessary to evaluate how the loads were distributed within the conveyor belt, how the stress concentrations developed in the welds, and how the conveyor belt responded under different Load Systems.

The effective notch method focuses on the local structural stresses using modeled notch radii. However, this method does not describe the global load distribution and is sensitive to mesh quality and complex geometry. The hot spot method primarily focuses on the structural stresses near the weld, where geometric discontinuities cause stress increases. This method does not fully capture the very local stress concentrations that develop at the weld root. The nominal stress method, on the other hand, evaluates the global stress level without considering local weld geometry. Therefore, comparisons between the results obtained from the different methods must be made with caution.

In the experimental test, the conveyor belt was subjected to a pure tensile load applied on one side of the belt. The finite element analyses were therefore designed to replicate these loading conditions as closely as possible.

3.2 Fatigue Life Assessment Approach according to Eurocode

According to Chapter 5 of Eurocode 3 Part 1–9 [26], fatigue verification shall be performed for steel structures. Two different verification concepts were defined. The first was the safe-life concept, which implied that the structure was designed so that fatigue failure was not expected to occur during the intended service life. The second concept is the damage-tolerant concept, which was based on the assumption that fatigue cracks could occur, but that the cracks would be detected and repaired before they could lead to failure.

Each steel structure consisted of several constructional details where local stress concentrations could occur. In Chapter 3.1.1 of Eurocode 3 Part 1-9 [26], different constructional details, such as welded joints and similar features, were identified. For each constructional detail, the most unfavorable potential crack initiation location was then

identified, for example at the weld root. This location subsequently governed the entire fatigue design.

The nominal stresses according to Chapter 7 of Eurocode 3 Part 1-9 [26] were calculated using a linear-elastic analysis. The nominal stress was defined as the elastic stress in the constructional detail while neglecting local stress concentrations. A stress range was then determined for the considered detail. In the case of constant-amplitude loading, the same stress range applied to all cycles. However, when variable-amplitude loading was present, cycle-counting methods such as the rainflow method may be required according to Eurocode 3 and Annex A [26].

In Chapters 8 and 10 of Eurocode 3 Part 1-9 [26], each constructional detail was classified and characterised by the characteristic reference stress $\Delta\sigma_C$. The fatigue life was then evaluated using the corresponding S–N curves defined by a specified slope parameter "m".

3.3 The Finite Element Model

In this thesis, finite element models were developed in ANSYS to analyse the fatigue life of the conveyor belts. The finite element models can be constructed using either shell or solid elements. In this study, only solid elements were used. The advantage of using solid elements was that they captured complex stress states more accurately. However, the main disadvantage was the increased computational cost.

3.3.1 Material Parameters

All components, including the welds, were made of steel and were assumed to behave in a linear-elastic manner. The standard material properties from ANSYS used in the finite element models are summarised in Table 3.1.

Table 3.1: Material Properties used in the finite element analysis for the conveyor belt components and welds.

Property of steel	**Value**	**Unit**
Density	7850	kg/m^3
Young's modulus	210×10^9	Pa
Poisson's ratio	0.3	–

3.3.2 Geometry

Below in Figure 3.1 the conveyor belt and its individual components are shown. The figure also includes the tension link. As will be mentioned later the analyses will be performed both with and without the tension link installed. The mesh net on which the products are transported on can also be seen. To simplify the finite element models, this component has not been included in the analyses.

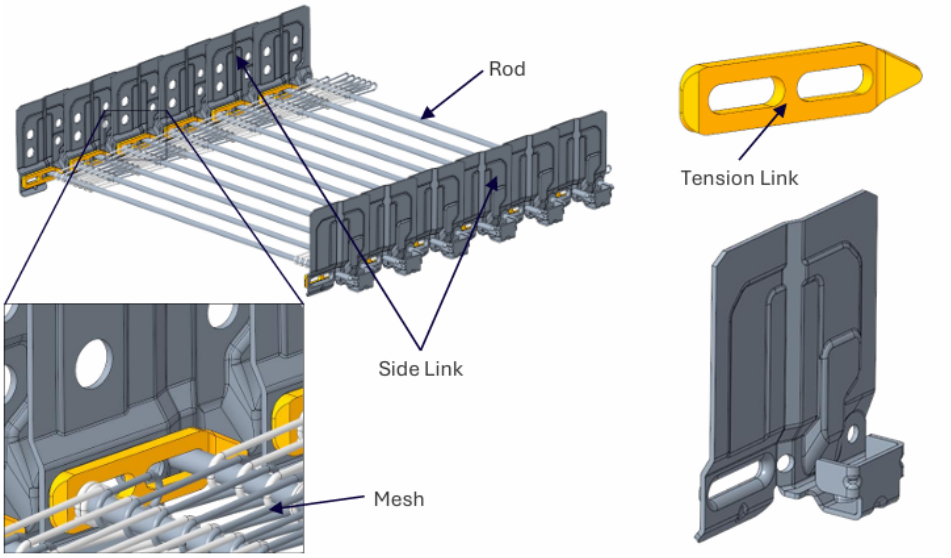

Figure 3.1: Overview of the conveyor belt, including tension link, side link, rods and mesh. In this case the tension link is included in the conveyor belt.

The thesis included two different conveyor belt designs, the Nova Belt and the Enhanced Nova Belt. The geometries of these two belts differed, as the enhanced version included an additional tension link. To reduce the computational cost, symmetry was utilised when constructing the finite element model, which allowed the model to be halved and later reduced to a even smaller number of side links. The finite element model is shown in Figure 3.2.

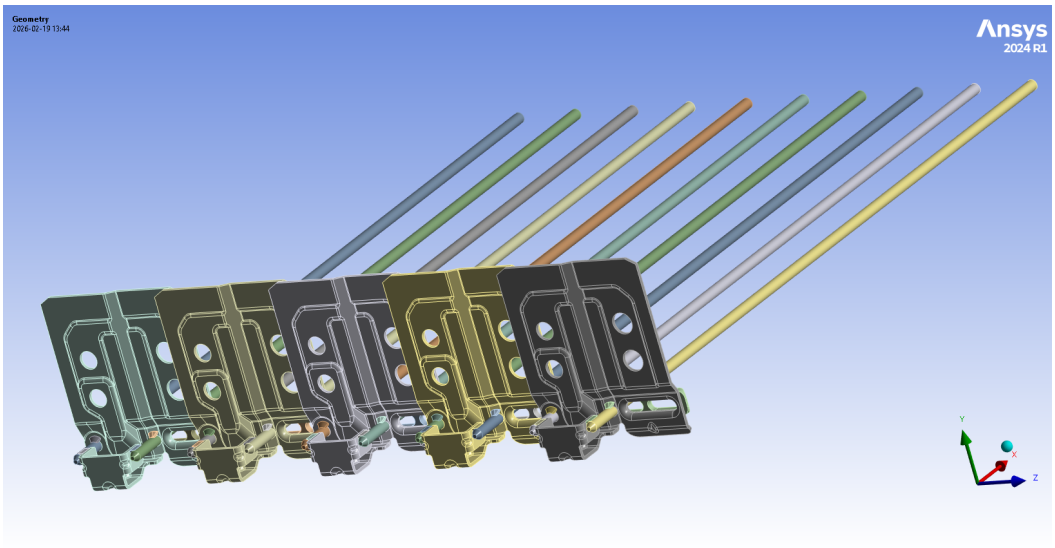

Figure 3.2: An overview of the geometry of the enhanced conveyor belt model including the side links, rods, tension link and welds used for the finite element analysis.

Nova Conveyor Belt

The Nova conveyor belt was made of two components, side links and rods, as shown in Figure 3.3. As mentioned previously, both the rods and the side links were modelled using solid elements.

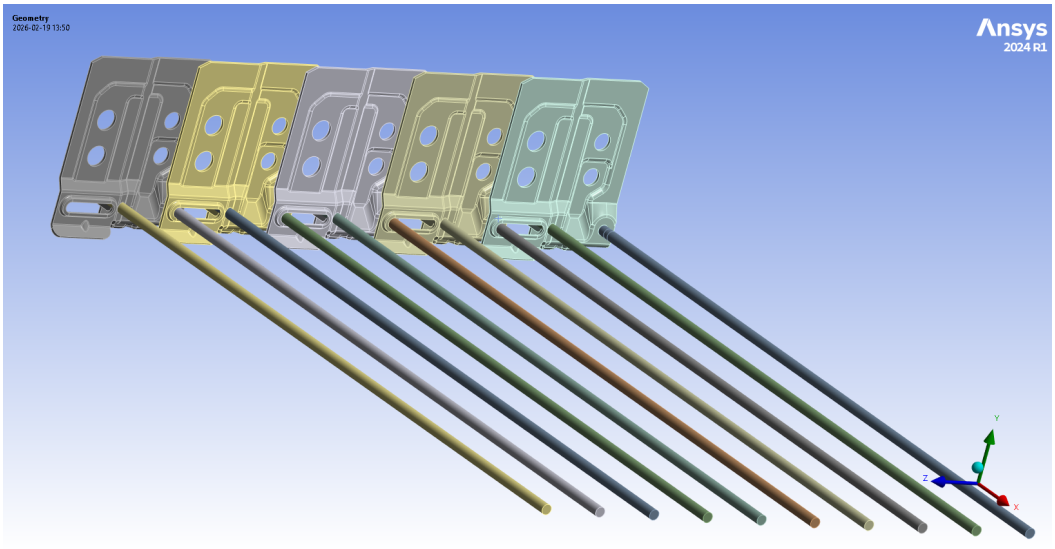

Figure 3.3: An overview of the geometry of the enhanced conveyor belt model including the side links, rods and welds used for the finite element analysis.

Enhanced Nova Conveyor Belt

The enhanced conveyor belt model was composed of three different parts, side links, rods, and an additional tension link. The tension links were positioned between two rods, as illustrated in Figure 3.4.

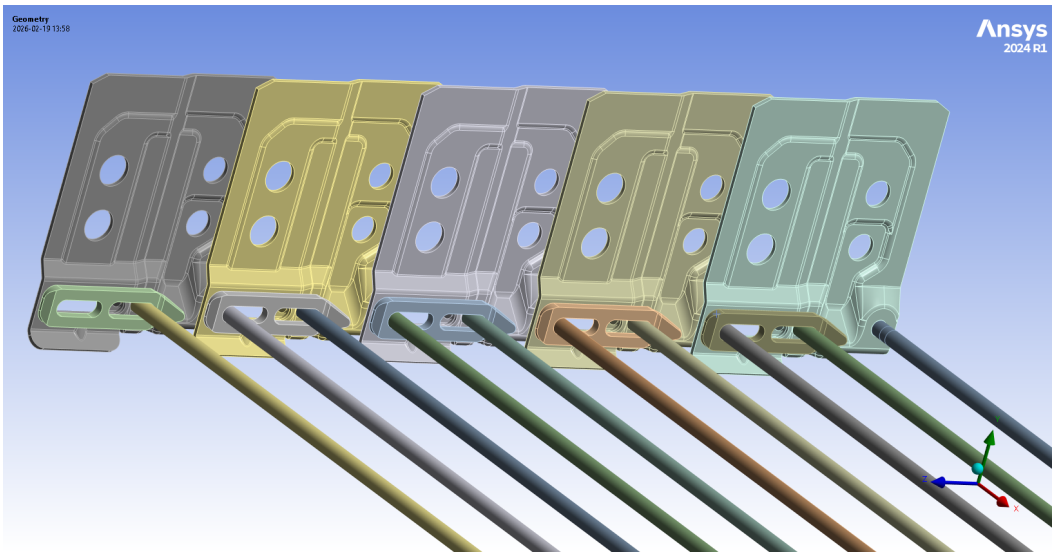

Figure 3.4: Geometry of the enhanced conveyor belt configuration where an tension link were introduced between the rods.

Geometry of Welds

The rods and side links were connected by four different welds. Two were located on the outer side of the vertical link (top welds), and the other two were located near the edge of the rod and connected to the side link foot. These welds were the only connections between these components, making them responsible for transmitting all applied loads between the rod and the side link. The welds, as well as the other components, were modeled using solid elements. In this thesis, only the upper left weld was analysed, as previous tests and investigations had shown that this was the most vulnerable weld. The different welds are shown in Figure 3.5.

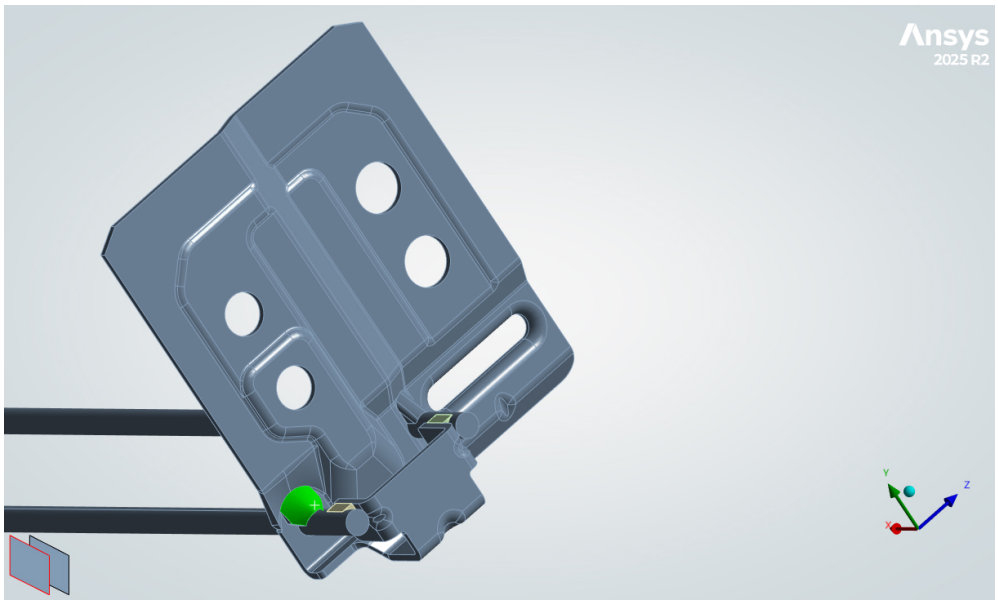

Figure 3.5: The figure shows the geometry of the different welds in the finite element model. Where the weld highlighted in green represents the weld investigated in this study.

The weld geometry was modeled to resemble the real weld geometry as closely as possible. Therefore, the top weld in the FEM model was rounded, as shown in Figure 3.5. The belt foot weld was constructed in such a way that it reflected the real belt. However, since this weld was not included in the analysis, its geometry was defined arbitrarily.

As shown in Figure 3.6, a 0,05 mm radius was introduced at the root of the weld. This was done according to the effective notch method [13].

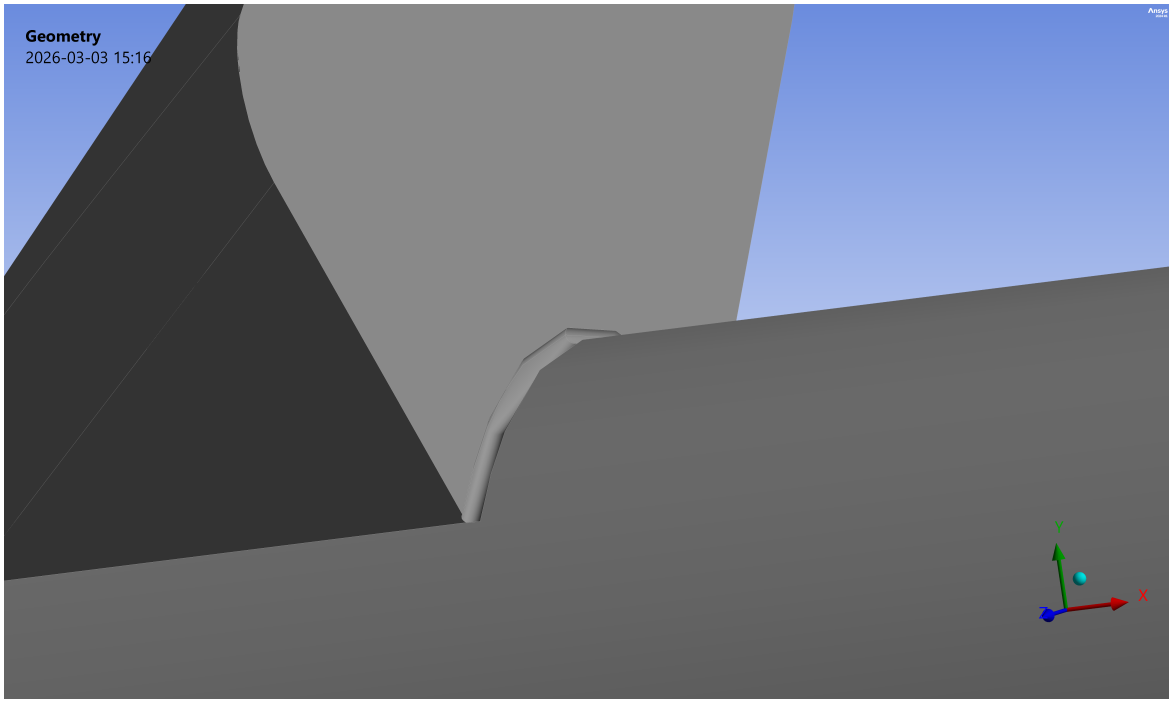

Figure 3.6: Illustration of how the notch radius is applied in the root of the weld in the finite element model. The figure shows the connection between the rod and weld and is seen without the side link included.

By introducing the notch radius in the finite element model the stress concentrations in the root converge towards a stable value. A notch radii of 1 mm is often used when calculating the effective notch stress. However, if this radii is inserted into the present model, too much material of the weld, side link, and rod is removed. Therefore, it is more suitable with a radii of 0,05 mm.

3.3.3 Mesh

According to IIW [11], the different parts of the model were meshed separately in order to obtain a finite element model that balanced accuracy and computational efficiency. A finer mesh was applied in the weld regions and at critical stress locations, while coarser meshes were used in areas away from the welds to reduce the computational cost. The coarse mesh consisted of high-order elements, for example 20-node isoparametric elements.

When using the effective notch stress method, the mesh size was chosen according to Table 2.2. In this case, the radii was set to 0.05 mm, and the element size for the

mesh around the radius was set to 0.008 mm. Further away from the notch radii, the mesh was coarser. This was done to reduce computation time, since this area was not of primary interest.

According to Table 2.2, the different meshing approaches that could be used to analyse welds using the effective notch method were presented. The weld being analysed was located on top of a rod. Therefore, tetrahedral elements with a quadratic formulation were used to obtain an appropriate representation of the weld regions. A mesh convergence study was performed to determine when the results for the welds of interest had converged.

To reduce the stress concentrations caused by meshing irregularities, the front weld, link, and rods were modelled as a single combined part. This approach ensured a smoother stress distribution. The applied mesh configurations for the combined geometry are illustrated in Figures 3.7 and 3.8.

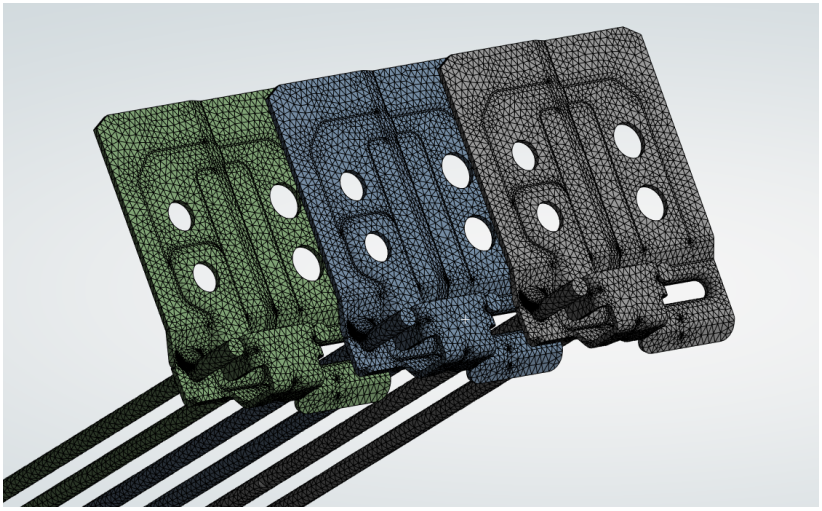

Figure 3.7: Mesh configuration used in the analysis. The rod, side link, and welds were meshed and modelled as one continuous part in order to achieve a smoother stress distribution.

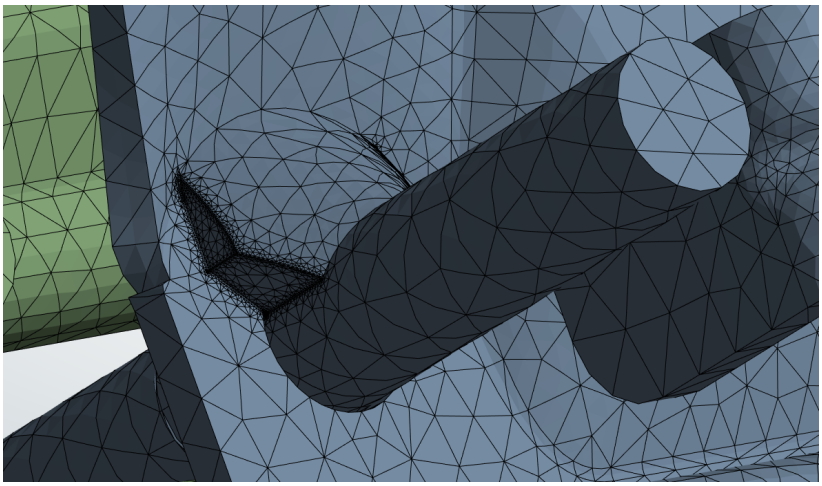

Figure 3.8: Fine mesh applied around critical weld regions in order to reduce stress concentrations caused by meshing irregularities.

A mesh convergence study was performed to ensure that reliable results were obtained. The study was conducted for Load System C, since it was the least computationally demanding load system. The convergence procedure was performed for both the effective notch method and the hot-spot method.

For the effective notch method, the maximum stress value at the notch was used to evaluate how the stress changed as the mesh was refined. A convergence study was performed by gradually reducing the surrounding element size and investigating how the stress varied, as seen in Figure 3.9. The element size at the notch radius was kept unchanged, since the selected element size already followed recommendations proved by IIW. Additional mesh refinements were not performed to keep the calculation time down. The mesh size was reduced down to 2mm for the effective notch.

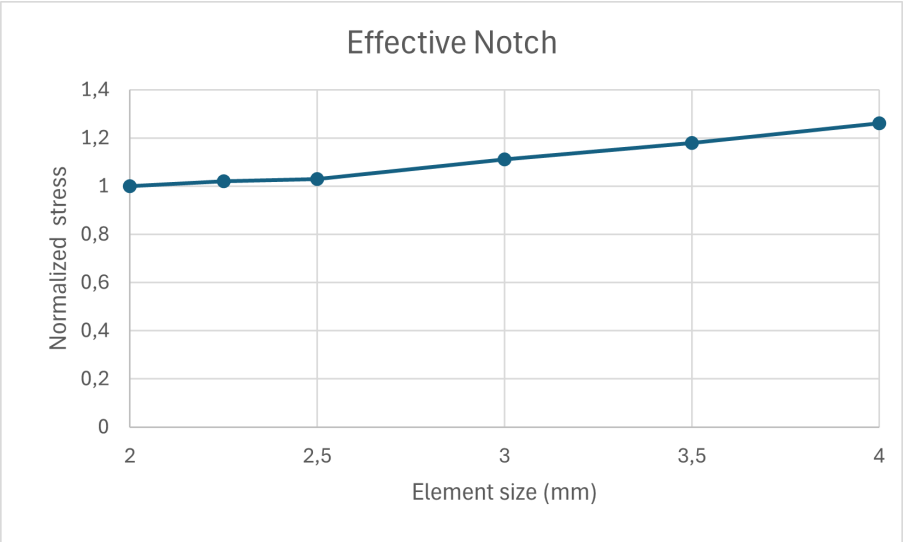

Figure 3.9: Mesh convergence study for the effective notch method. The normalized stress values are slowly decreased and approach a stable result, indicating that the selected mesh size provides a stable accuracy for the result.

For the hot-spot method, a reference point located at a distance of 1,0t from the weld root was used to evaluate how the stress varied with mesh refinement. Since the side link, rod and welds was modelled as one part. The element size of the entire component was gradually reduced until the stress variation became smaller and more stable. The stress value converged when the mesh was 1 mm, as seen in Figure 3.10.

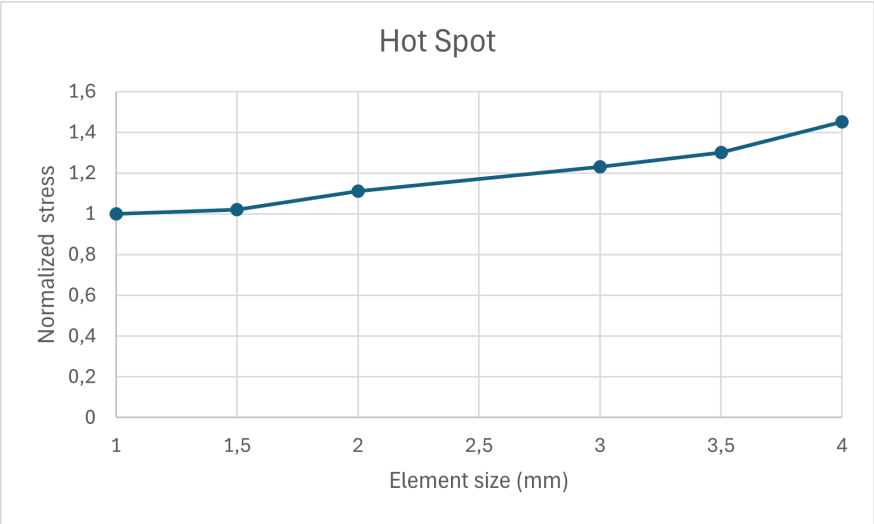

Figure 3.10: Mesh convergence study for the hot-spot method. The stresses extracted at the reference point become more stable as the mesh is refined, indicating convergence of system.

3.4 Load Systems

As the belt moved through the freezer, it was subjected to varying loading conditions. These loading conditions could be broadly categorized into two main load types: belt tension and vertical loading. The forces acting on the bottom layer of the belt are shown in Figure 3.11, which also illustrates the regions in the freezer where the products were located on the belt. Within the stack, the combined weight of the products and the belt induced bending in the rods, which were constrained by the side links on the tier above.

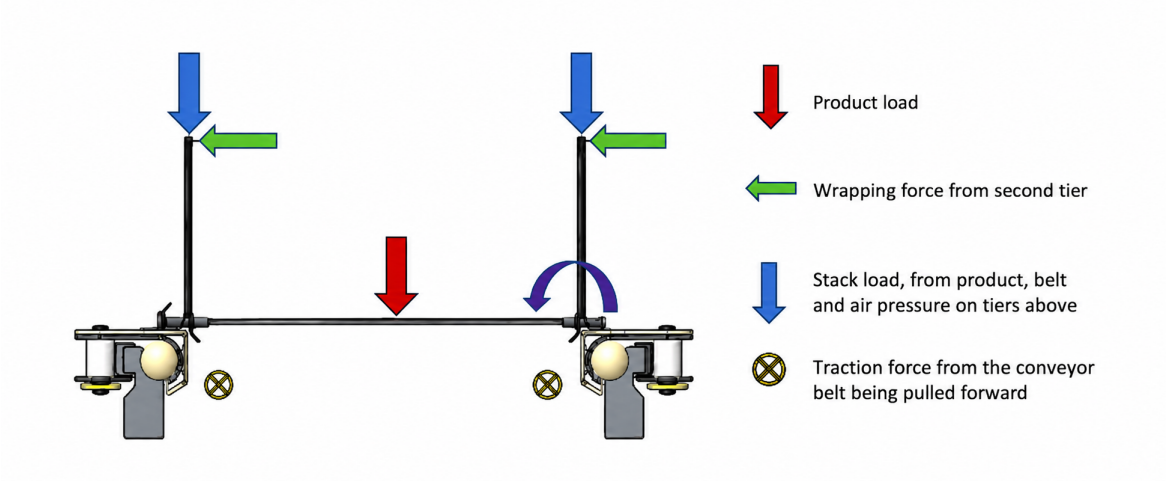

Figure 3.11: Illustration of how the different loads acted on the conveyor belt. The product load acted vertically on the rods. The stack and wrapping forces acted on the top of the side link, while the tension force acted on the belt foot.

In this study, only the vertical load from stacking, the belt tension, and the product load acting on the rods were considered. The wrapping force was neglected. The vertical load and the stacking load vary over time due to the operating conditions of the conveyor system, whereas the product load was assumed to remain constant throughout the analysis.

3.4.1 Load System A – Belt tension Without a Tension Link

In Load System A, the conveyor belt was subjected only to the tension force arising from the drive system and the friction forces between the belt and the supporting structure as the belt was pulled through the freezer. To reduce computational cost, the model was limited to three side links in this Load System.

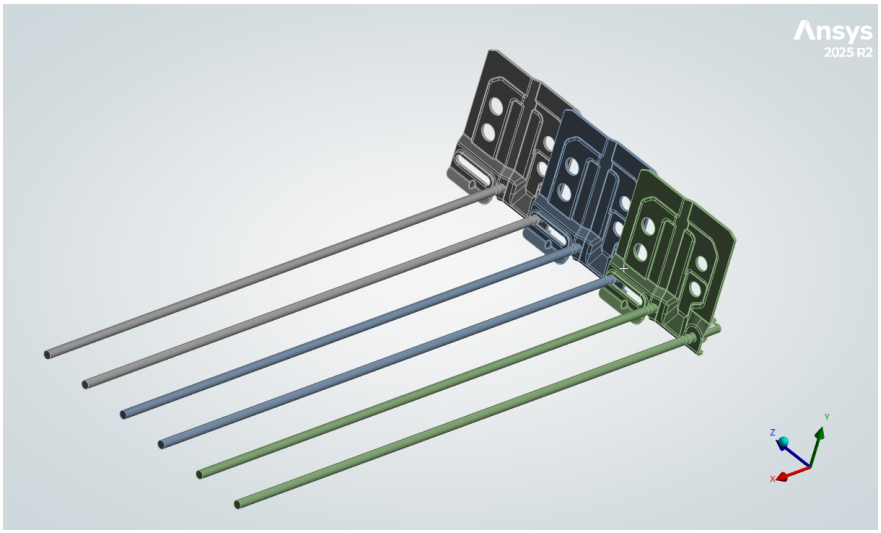

Figure 3.12: Finite element model of Load System A, where the conveyor belt is subjected to tensile loading without tension link.

In the finite element model, this force was applied to the surface area of the rod where the next side link was intended to be placed. In this way, a model was obtained that corresponded to the real-life situation. The tensile force was then scaled linearly using step cycles. In Figure 3.13, illustrates how the force was applied.

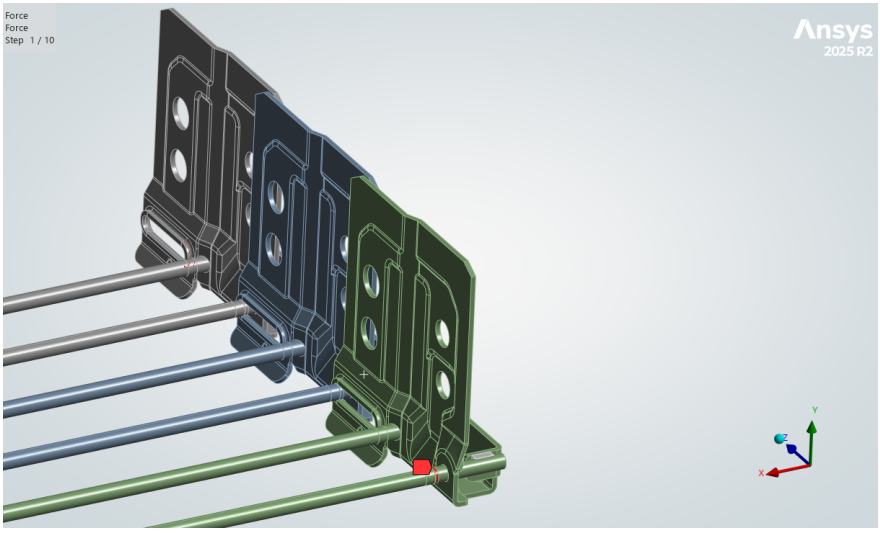

Figure 3.13: Illustration of the applied tensile loading used for Load System A in the finite element analysis.

The tensile force acting on the conveyor belt varied. To represent different operating conditions, seven load steps were defined. The maximum force for each load step was increased according to the normalised force shown in Figure 3.14. Each load step represents a different force range used in the fatigue analysis.

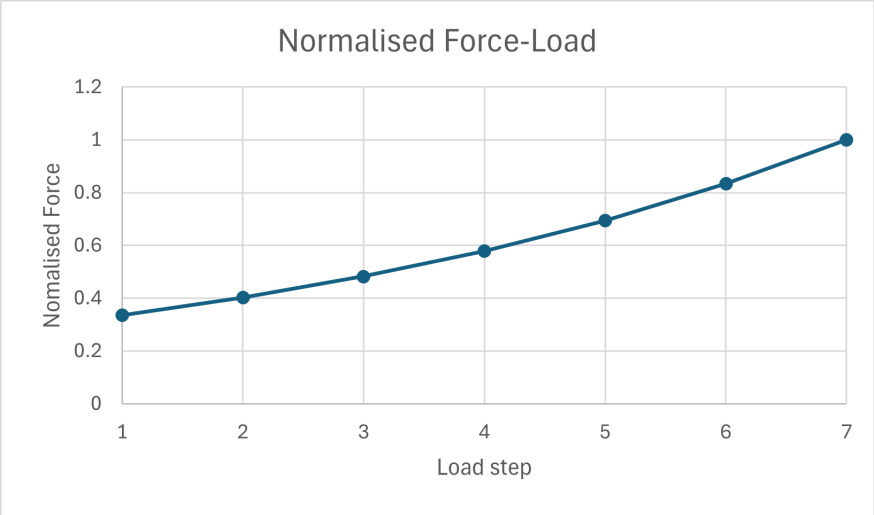

Figure 3.14: Seven different normalised force levels used in the finite element analysis of Load System A and B, scaled linearly with a 20% increase between each load step.

Boundary Conditions – Load System A

Load System A was subjected only to a tensile force, which required appropriate boundary conditions to represent the real-life structure. In reality, the belt consisted of a large number of side links arranged in series, but in this case the model was limited to three links. Therefore, the model was restrained against displacement at the last side link in the same direction as the applied force, as shown in Figure 3.13.

An additional boundary condition was applied at the belt foot, where translation in the y-direction was constrained, as shown in Figure 3.15a. Finally, a symmetry boundary condition was applied at the ends of the rods since the model was halved, as shown in Figure 3.15.

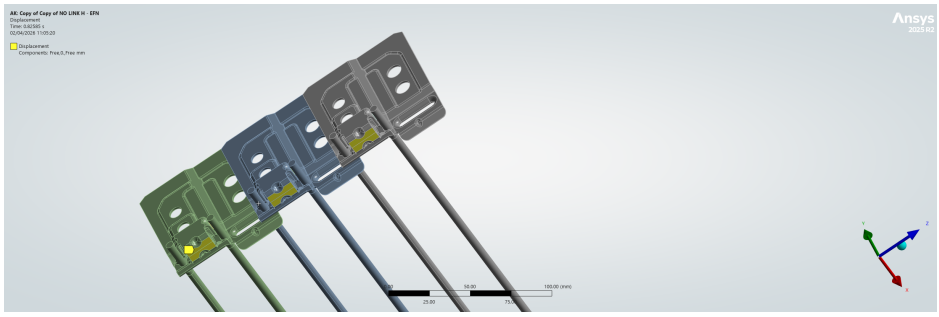

(a) Boundary condition used in the finite element model where the belt foot was prevented from moving in the Y-direction.

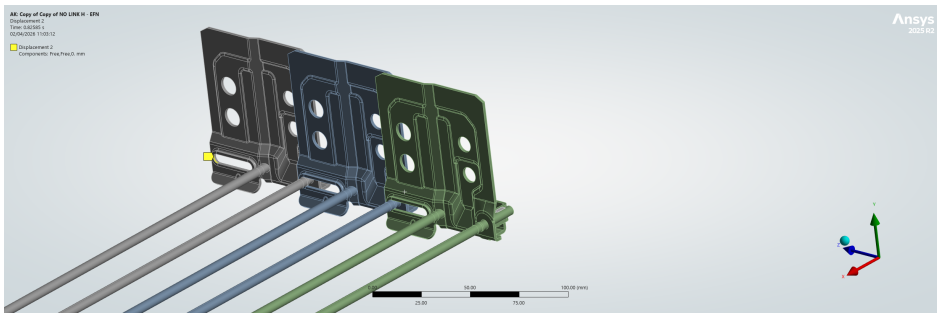

(b) The final side link was constrained in the loading direction in order to prevent rigid body motion of the model.

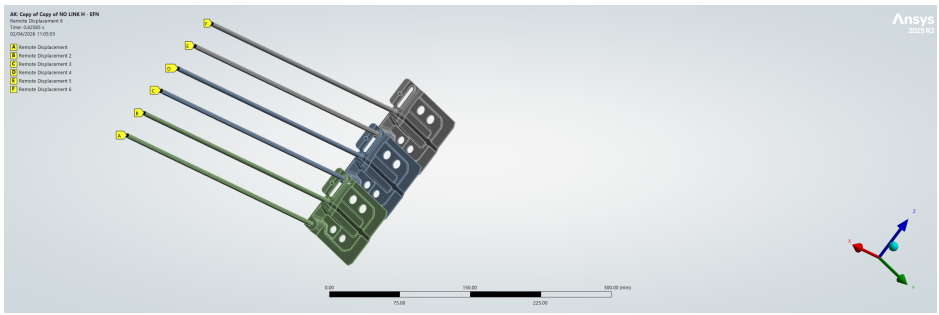

(c) Symmetry boundary conditions were applied in the YZ-plane to represent half of the conveyor belt model in the analysis.

Figure 3.15: Boundary conditions used for Load System A.

Connections – Load System A

For Load System A, different connections were defined. A rigid contact was applied between the weld, side link and rod, causing them to share topology and behave as a single component. Between the rod and the oval hole, a frictional contact was defined. This type of contact allowed the two components to remain in contact until the friction limit was reached, after which sliding could occur, as illustrated in Figure 3.16.

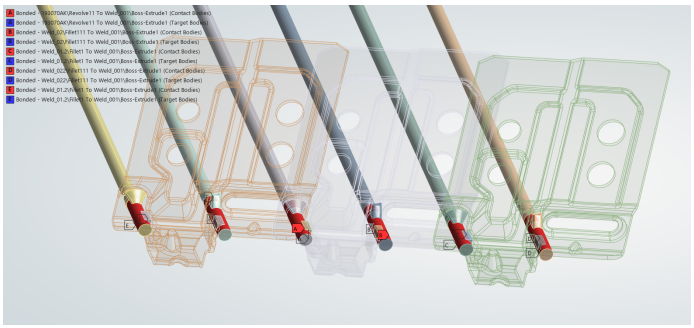

(a) Rigid contact between rod and link – back.

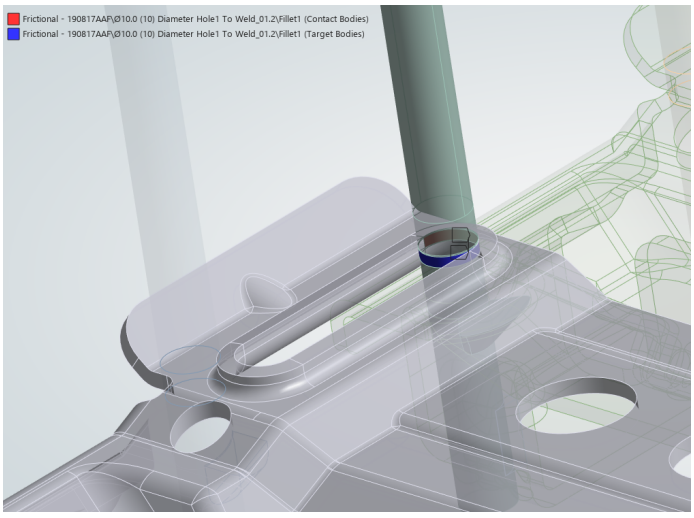

(b) Frictional contact between side link and the rod at the oval hole.

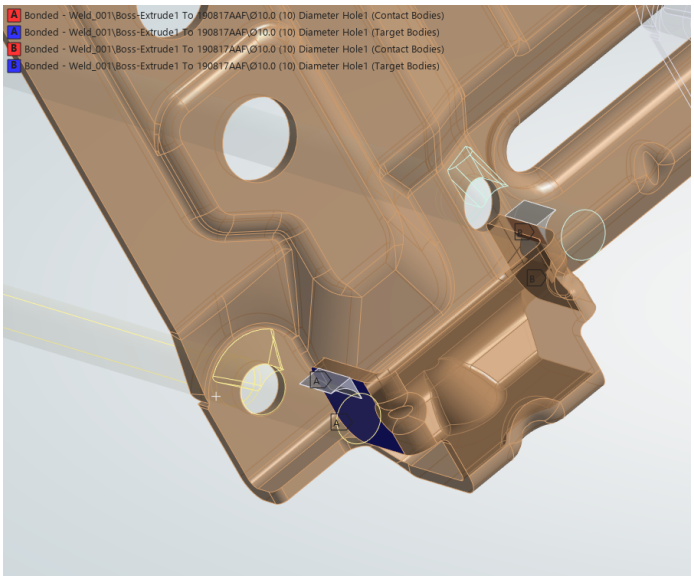

(c) Rigid contact between weld and link – back.

Figure 3.16: Connections used for Load System A in the finite element model.

3.4.2 Load System B – Belt Tension with Tension Link

For Load System B, the model was reduced to only three side links, since the enhanced Nova belt with tension links was considered. The finite element model used in the analysis is illustrated in Figure 3.17.

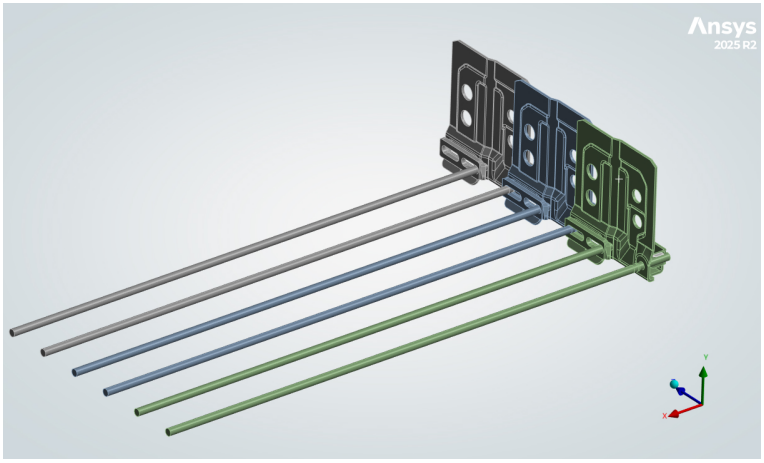

Figure 3.17: Finite element model used for Load System B, including the tension link in the conveyor belt system.

Since tension links were included, the force was applied at the last rod where the tension link would normally have been located. The tensile force was then scaled linearly using step cycles. Figure 3.18 illustrates how the force was applied. The evaluated stress was the von Mises stress, which was used for fatigue life evaluation.

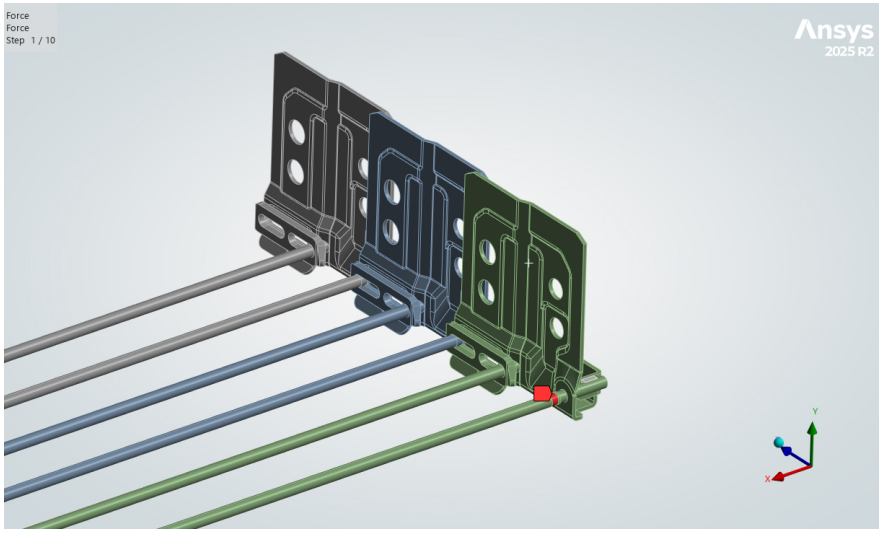

Figure 3.18: Illustration of applied tensile loading used for Load System B in the finite element analysis.

The load was applied in the same manner as in Load System A, see Figure 3.14.

Boundary Conditions – Load System B

Load System B used the same boundary conditions as Load System A. However, instead of restraining the first side link against displacement in the z-direction, the first tension link was restrained, as shown in Figure 3.19.

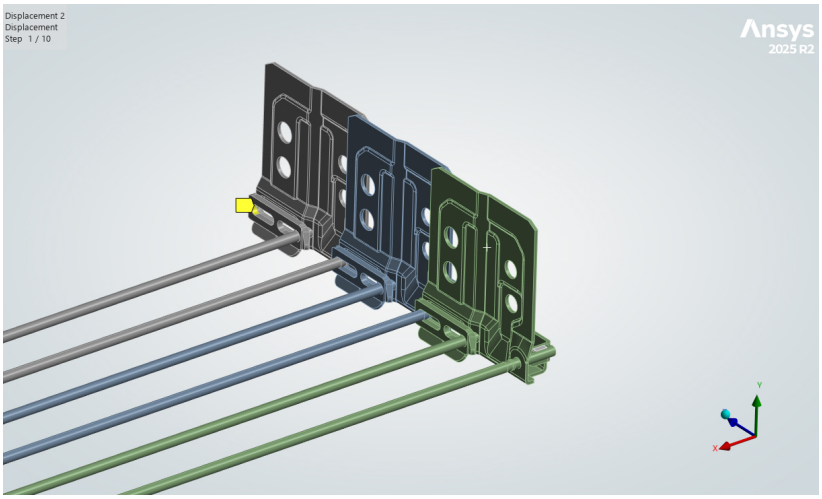

Figure 3.19: The model restrained from movement in the loading direction (Z-direction) by fixing the last tension link.

Connections – Load System B

The connections for Load System B were the same as those used Load System A. The only difference was that the frictional contact at the oval hole was replaced by a frictional contact at the tension link. This meant that no frictional connection existed between the rod and the side link. The new frictional contact is illustrated in Figure 3.20. This contact was defined between all tension links and the corresponding rods.

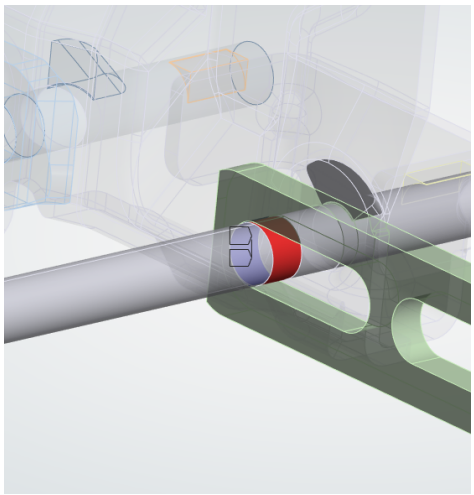

Figure 3.20: Frictional contact defined between tension link and the rod in the finite element model.

3.4.3 Load System C – Vertical Load without Tension Link

In Load System C, the vertical force was applied to a model without a tension link. The model was reduced to an analysis of a single side link, as illustrated in Figure 3.21.

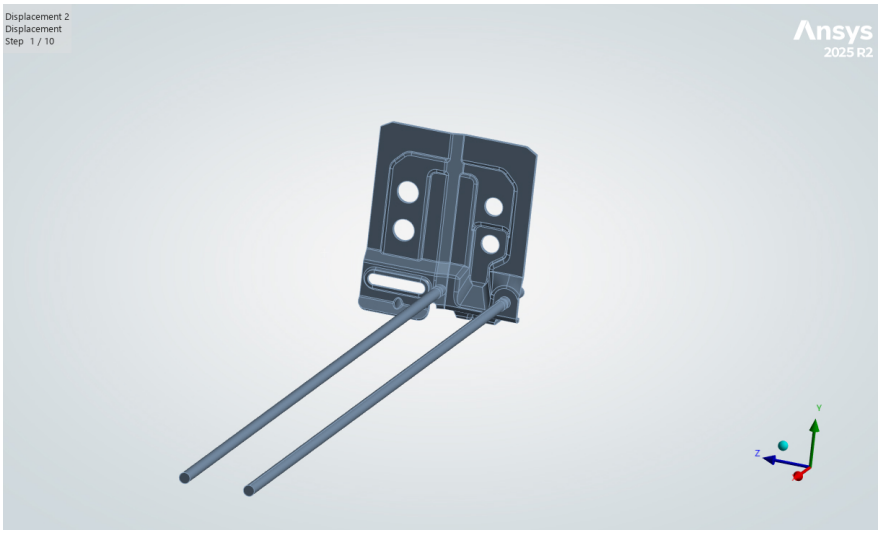

Figure 3.21: Finite element model used for Load System C, where the conveyor belt was subjected to vertical loading.

The force was applied on top of the side link, representing the stack load as seen in Figure 3.22. The product load is applied as a line load along the upper part of the rods to represent the weight of the product, as seen in Figure 3.23

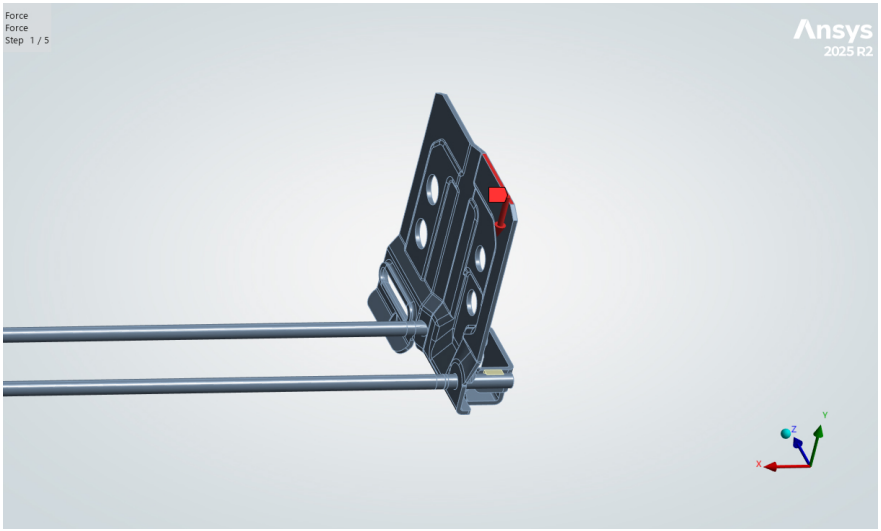

Figure 3.22: The vertical force applied on top of the side link to represent the stack load on the conveyor belt.

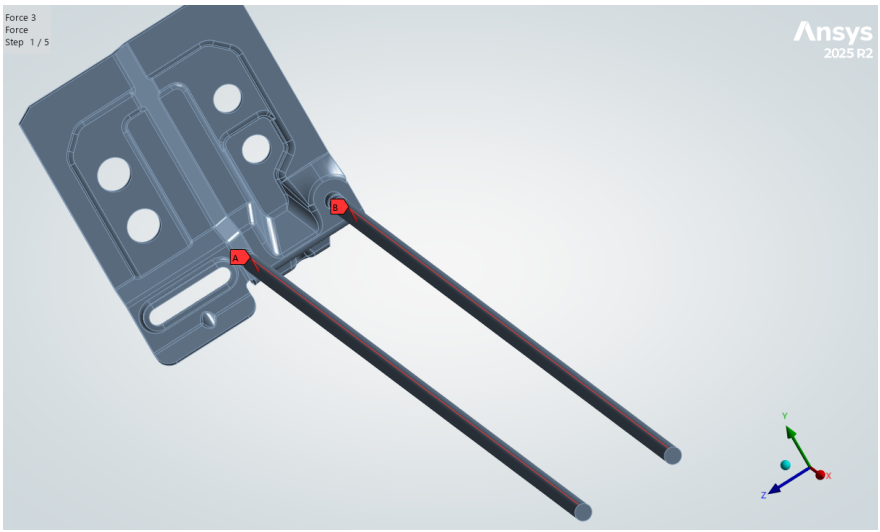

Figure 3.23: Illustration of the distributed loading condition used to represent the product weight acting on the rods at Points A and B used in Load System C. This force maintained at the same magnitude throughout all load steps.

In this load system, five different cyclic forces were applied at the top of the side link, as seen in Figure 3.22. In Figure 3.24 the maximum normalised force for each force range is illustrated. These five forces were selected according to the information provided by JBT Marel.

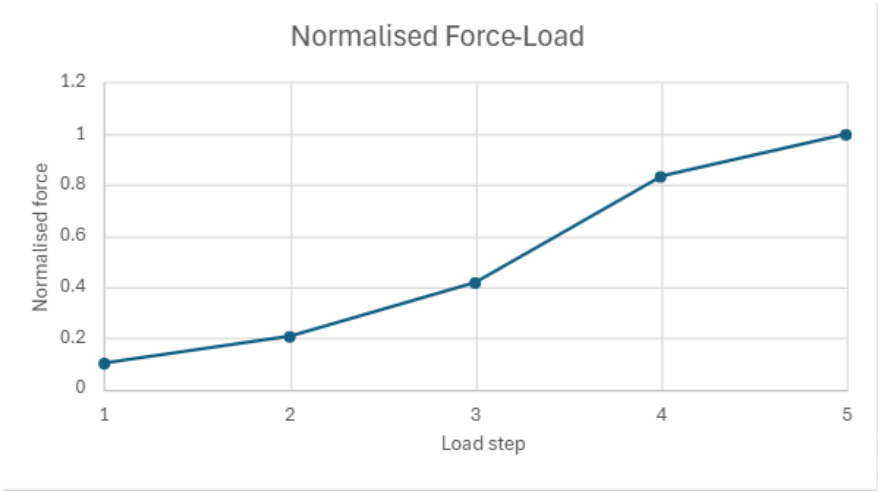

Figure 3.24: Five different loads applied in the finite element analysis of Load System C, with increasing load magnitude for each step.

In addition to the vertical load applied to the side link, the product load acting on the rods was also included, as shown in Figure 3.23. This force was constant for all load steps and corresponds to the heaviest product transported on the conveyor belt. The resulting stress contribution from this load was almost negligible, therefore no lower loads were analysed.

Boundary Conditions – Load System C

Several boundary conditions were applied in Load System C. Similar to the other models, symmetry boundary conditions were used at the center of the belt, in order to reduce the computational cost. In addition, the belt foot was constrained against translation in the y-direction, as illustrated in Figure 3.25.

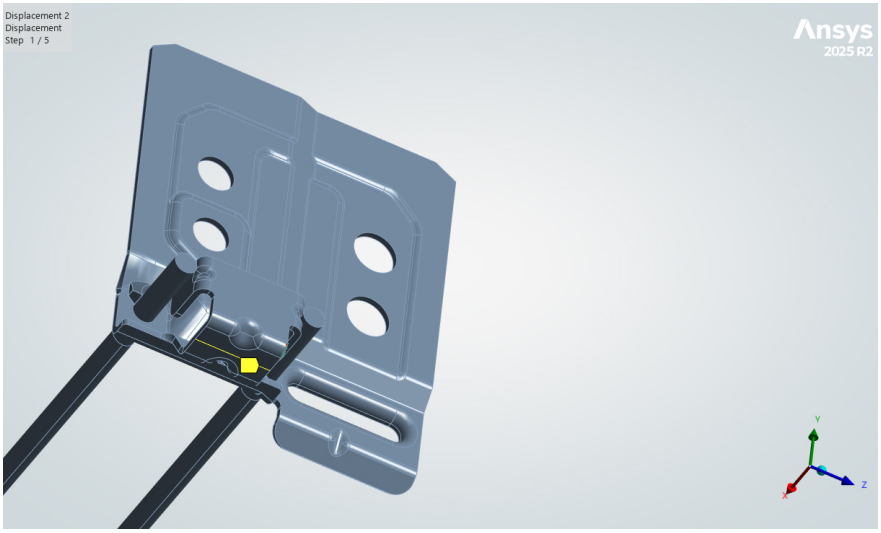

Figure 3.25: The belt foot is constrained from translation in y-direction beneath the side link foot in the finite element model.

Furthermore, a small section on the side of the side link was constrained in the z-direction. The upper edge of the side link was also partially constrained, where a small line at the top was fixed in the x-direction. See Figure 3.26.

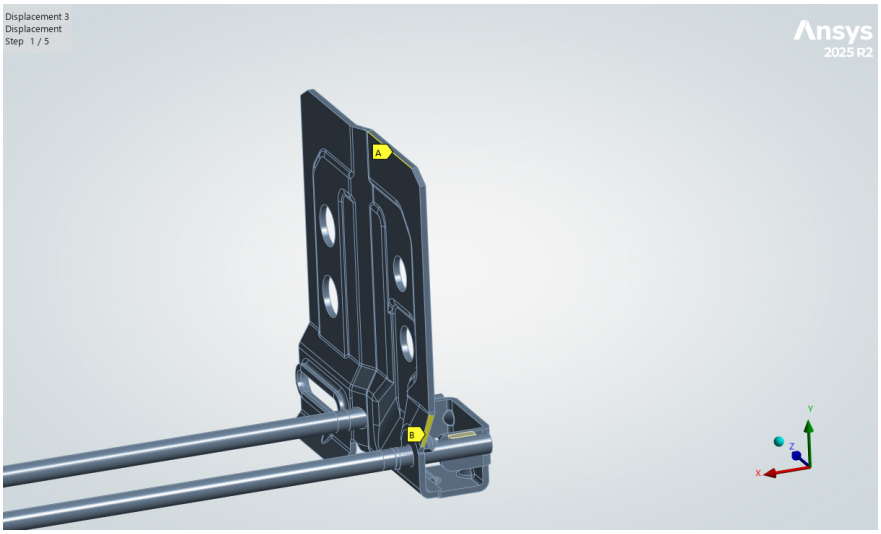

Figure 3.26: Illustrating of the boundary conditions used to constrain the model in the x-direction at Point A and in the z-direction at Point B.

Connections - Load System C

The connections for Load System C are made in the same manner as presented in 3.4.1 for Load System A. The connections for Load System C are illustrated in Figure 3.27.

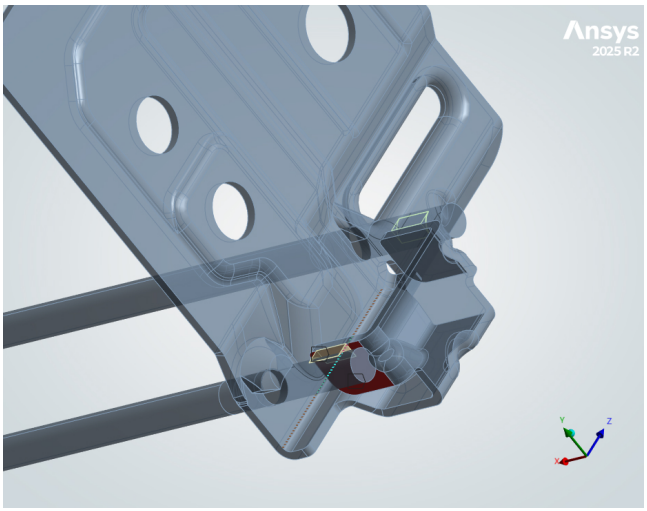

(a) Connection between the weld and link in the back.

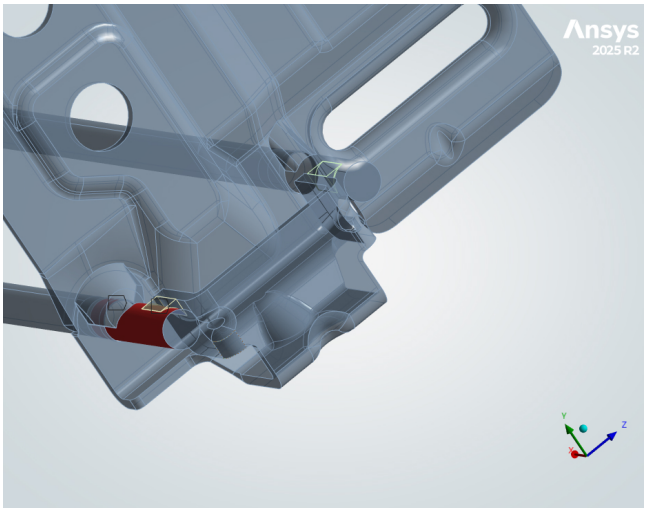

(b) Connection between rod to weld in the back.

Figure 3.27: Connections used in the finite element model for Load System C.

3.5 Calculation of Fatigue Life

The fatigue life was calculated according to Eurocode 3 Part 1-9: Fatigue [26]. The following relation was used. See Equation 3.1.

$$N_i = N_c \cdot (\frac{\Delta\sigma_c}{\Delta\sigma_i})^m \tag{3.1}$$

Where $\Delta\sigma_c$ represented the characteristic fatigue strength at 2×10^6 cycles, m was the slope of the resistance curve, $\Delta\sigma$ denoted the stress range and N_c was the reference number of cycles. The value of $\Delta\sigma_c$ was selected according to the relevant detail category, as presented in Table 4.1. The stress range was then determined using either analytical or computational methods. The slope parameter m was obtained from the S–N curves corresponding to the chosen detail categories. By using this expression, the fatigue life N_i for each stress cycle could be calculated.

3.6 Calculation of Nominal Stress

In this thesis, the nominal stress was determined using analytical calculations according to Eurocode part 1-9 [26].

The stress state in the weld was evaluated for a tension-loaded connection both with and without a tension link. Both direct loading and the effect of load eccentricity were considered. The following parameters were selected to represent those used in the finite element model allowing a comparison between the different calculation methods.

a	Throat thickness
L	Weld length
F	Applied force
e	Eccentricity

The effective weld area is given:

$$A = a \cdot L \tag{3.2}$$

The direct shear stress acting on the weld due to the applied force is calculated as:

$$\tau = \frac{F}{A} \tag{3.3}$$

An eccentric load introduces an additional bending moment, defined as:

$$M = F \cdot e \tag{3.4}$$

The weld is treated as a line element with throat thickness a. The bending stress is calculated based on the second moment of area of the weld group:

$$\sigma_b = \frac{M \cdot y}{I} \tag{3.5}$$

where y is the distance from the neutral axis to the point of interest, and I is the moment of inertia of the weld.

The nominal stress is obtained by superimposing the direct and bending stress contributions:

$$\sigma_{\text{nom}} = \frac{F}{A} + \frac{M \cdot y}{I} \tag{3.6}$$

3.7 Factor for Reduction of Loads Applied to Load System C

After the vertical load system without a tension link had been evaluated, Miner's rule was used to derive a reduction factor. According to [26], Miner's rule was described as a method for calculating cumulative fatigue damage. It was used to estimate fatigue damage under variable amplitude loading. The method assumed that each stress level contributed to the total fatigue damage and that these contributions could be added linearly.

For different load steps divided into k stress levels, the accumulated damage was defined as

$$D = \sum_{i=1}^{k} \frac{n_i}{N_i}, \tag{3.7}$$

where n_i was the number of cycles applied at stress level i, and N_i was the number of cycles to failure at the same stress level according to the selected S–N curve.

Failure was assumed to occur when the accumulated damage reached

$$D \geq 1. \tag{3.8}$$

From the finite element method analysis of the Load Systems A and B with horisontal loading, a reduction factor was obtained by scaling the stresses until the predicted fatigue life matched the experimental data from the conveyor belt tests performed by JBT. This reduction factor was then applied to Load System C, which represented the vertical load system.

By applying this factor, a more representative estimate of the actual fatigue life of the conveyor belt was obtained.

3.8 Parameter study – Load System A

A parameter study was carried out using the effective notch method by varying the weld throat dimension, as illustrated in Figure 3.28. The parameter study was performed for Load System A as this load system produced the highest stresses in the weld from previous analyses in this study. First a reference model was created. The weld throat was then reduced by 0.5 mm and increased by 0.5 mm in separate analyses. After each modification the simulation was run again to evaluate how the stresses changed.

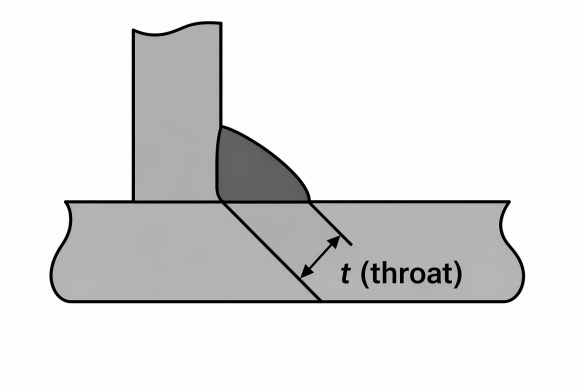

Figure 3.28: Illustration showing the weld throat. The throat represent the shortest distance between the weld root and the weld face [20]. The weld throat dimension was varied in the parameter study by increasing and decreasing the size.

3.9 Bilinear Isotropic Hardening – Load System B

For Load System B, a plastic analysis using bilinear isotropic hardening material was performed. The procedure consisted of first loading the model using the nonlinear material properties until the desired load level was reached. The structure was then unloaded and the displacements from the unloading step were extracted. These displacements were mapped onto a second model with purely elastic material properties, which was solved again. The results from the elastic and plastic analyses were then compared. This procedure was carried out for three load steps. The material properties used in the bilinear isotropic hardening model are summarised in Table 3.2.

Table 3.2: Material data used for bilinear isotropic hardening model in the finite element analysis. The material model includes the yield strength and tangent modulus used to represent the plastic behavior of the steel after yielding.

Parameter	**Value**
Tangent Modulus Type	Plastic
Yield Strength	$2.5 \cdot 10^8$ Pa
Tangent Modulus	$2 \cdot 10^8$ Pa

3.10 Analysis of Large Deflection – Load System B

An investigation of whether large deflection affected the result was also carried out using the effective notch stress method for Load System B.

Large deflection means that the stiffness matrix of the system is updated as the structure deforms. This enables accurate simulation of large displacements, significant rotations, stress stiffening, and buckling. These effects cannot be captured using linear analysis which assumes small deformations and linear behavior. The equation used in the finite element method is given by [27]:

$$\mathbf{Ka} = \mathbf{f} \tag{3.9}$$

where

$\mathbf{K}$ = the stiffness matrix, $\mathbf{a}$ = the nodal displacements, $\mathbf{f}$ = the applied load.

3.11 Generative AI

Artificial intelligence (AI) was used as a support tool to improve the language and structure of the text. With the aim of enhancing clarity and readability. All suggested improvements were carefully reviewed to ensure that the intended meaning of the text was preserved. AI was also used to help identify relevant theoretical topics for the study. All material suggested by ai was carefully reviewed and verified. The use of AI provided an additional perspective on which theoretical aspects were relevant, both for the study that was conducted and for providing a sufficient theoretical foundation for the proposed future studies.

AI was also used to generate figures based on specified requirements, which were subsequently reviewed to ensure accuracy and quality.

4 Fatigue Life Assessment

In the following chapter, fatigue life assessments were performed for the different Load Systems. The corresponding FAT classes for the different evaluation methods are presented in Table 4.1.

Table 4.1: Different FAT - classes used for the evaluated fatigue assessment methods in the study. The selected FAT classes were chosen based on weld geometry and recommendations from IIW and Eurocode [11], [26].

	Effective notch	Hot spot	Nominal stress
FAT class [MPa]	630	100	80

All presented stress values, as well as comparisons between stress values, were based on the von Mises stresses. This was because the applied loading conditions satisfied the requirements for using the von Mises stress criterion rather than the maximum principal stress criterion, which could only be applied if specific conditions were fulfilled.

4.1 Fatigue Life – Load System A

Fatigue life calculations were performed for Load System A, which concerns a conveyor belt without a tension link. In this case, seven different load levels were used.

4.1.1 Real-life Testings and Theoretical Fatigue Results

Experimental testing was conducted by JBT Marel. During the experimental testing, seven different load steps were applied. At each load step, a specified number of cycles was performed. Failure of the conveyor belt occurred during the seventh load step.

The experimental results are compared with the analytical results obtained using the effective notch, hot spot, and nominal stress methods. A summary of the performance of the different methods is presented in Table 4.2.

A value below 100% indicates that the predicted stresses are lower than those observed in the experimental testing, implying an overestimation of fatigue life. Meanwhile, a value above 100% indicates that the predicted stresses are higher, corresponding to a more conservative estimation of the fatigue life.

The table was created by scaling the stresses for each method by a constant factor so that all methods reached failure during the same final load step as observed in the experimental test. Miners rule was then used to calculate the number of stress cycles for each load step, to determine the number of cycles required for each method to

reach failure. The calculated value for each method was then compared to the original result for each method. This made it possible to evaluate how closely each method predicted the fatigue life observed in the experimental test data. Since the result was scaled linearly but the load also varied linearly, there is very little variation in the result between the different load steps.

Table 4.2: Comparison between the aim value and the evaluated fatigue life results for the different stress assessment methods at each load step. The table shows how the effective notch, hot-spot, and nominal stress methods differ in their predicted fatigue response relative to the aim value of 100%.

Load step	Aim value	Effective notch	Hot spot	Nominal stress
1	100%	344.86%	74,11%	60,23%
2	100%	348,56%	74,21%	60,23%
3	100%	351,26%	74,28%	60,23%
4	100%	353,10%	74,28%	60,23%
5	100%	354,23%	74,18%	60,23%
6	100%	354,85%	74,07%	60,23%
7	100%	355,06%	74,65%	60,23%

4.1.2 Fatigue Life Evaluation

The fatigue life calculations were based on three different stress evaluation methods, the effective notch-, hot spot-, and nominal-stress method. For the hot spot and effective notch stress methods, stresses are evaluated using the finite element method in ANSYS, whereas nominal stress calculations were calculated analytically.

For the different methods, the S-N curves were plotted separately using logarithmic axes. Both the stress and life cycle values were normalized by dividing the evaluated values by a constant. All results are presented in Figure 4.1a, 4.1b and 4.1c for the different evaluation methods. In these plots, load step one is located on the far right, with subsequent load steps positioned progressively to the left, while the values of the stress increase as the stress levels increase

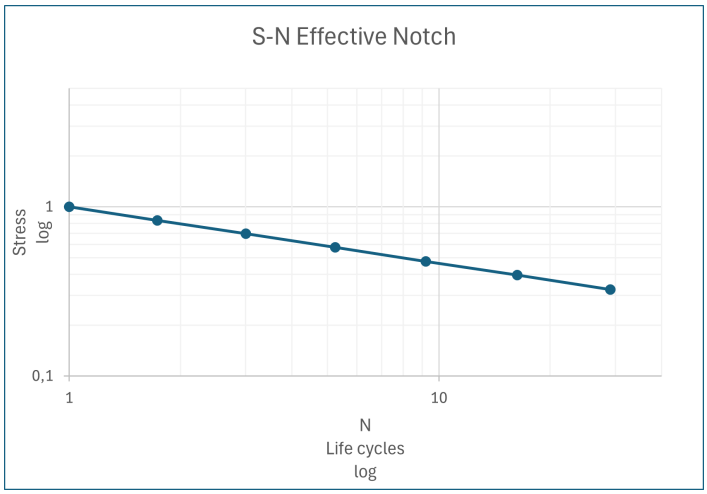

(a) Calculated S-N curve for the effective notch method.

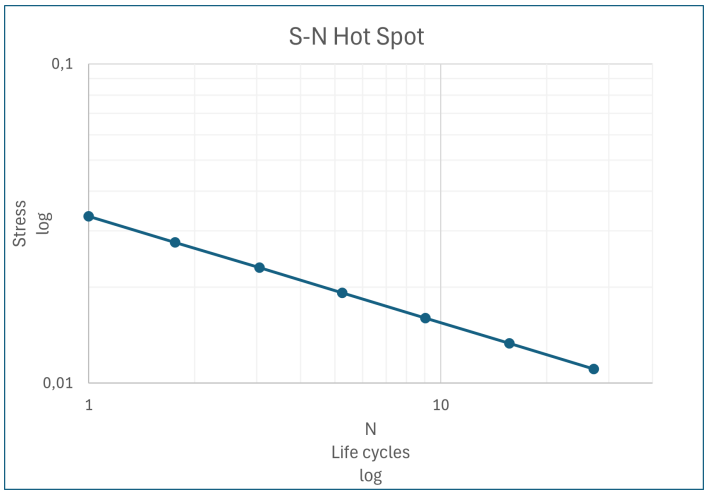

(b) Calculated S-N curve for the hot spot method.

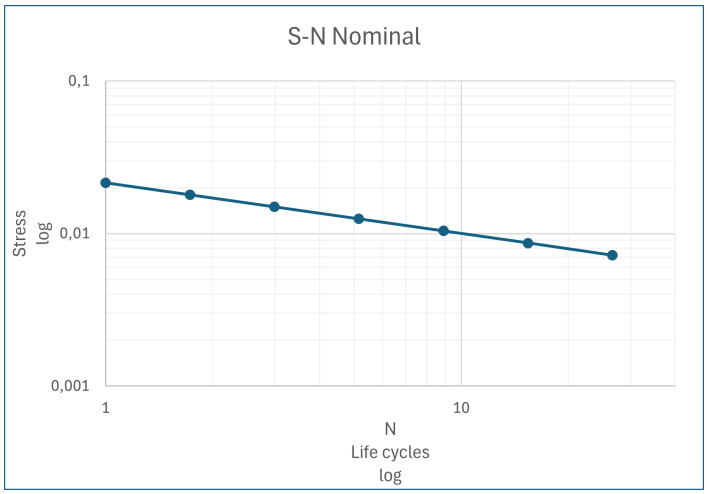

(c) Calculated S-N curve for the nominal method.

Figure 4.1: Normalized S–N curves for the different fatigue evaluation methods used in the study for Load System A. The curves are based on the selected FAT classes and describes the relationship between stress and number of cycles to failure. The calculated values were then normalized using a constant.

4.2 Fatigue life – Load System B

The same procedure as that used for Load System A was applied to Load System B. In this case, a tension link was included. The same FAT–classes are used as those presented in Table 4.1

4.2.1 Real-life Testings and Theoretical Fatigue Results

A summary of the performance of the different methods i presented in Table 4.3. The table shows how far from 100% the different methods are. The comparison presented in Table 4.3 follows the same approach as Table 4.2.

Table 4.3: Comparison between the aim value and the evaluated fatigue life results for the different stress assessment methods at each load step. The table shows how the effective notch, hot-spot, and nominal stress methods differ in their predicted fatigue life relative to the aim value of 100%.

Load step	Aim value	Effective notch	Hot spot	Nominal
1	100%	337,09%	61,29%	122,98%
2	100%	341,42%	61,15%	122,98%
3	100%	345,02%	60,89%	122,98%
4	100%	348,02%	60,81%	122,98%
5	100%	350,52%	60,82%	122,98%
6	100%	352,60%	60,79%	122,98%
7	100%	351,24%	61,12%	122,98%

4.2.2 Fatigue Life Evaluation

The S-N curves were constructed in the same way as in Load System A. The values were normalized by dividing them by a constant and different methods were then plotted separately using logarithmic axes. The results are presented in Figures 4.2a, 4.2b and 4.2c, showing the relationship between stress and the corresponding number of life cycles.

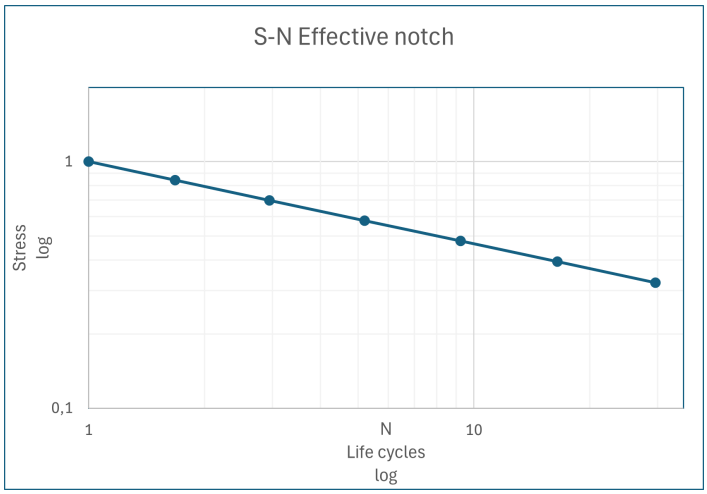

(a) Calculated S-N curve for the effective notch method.

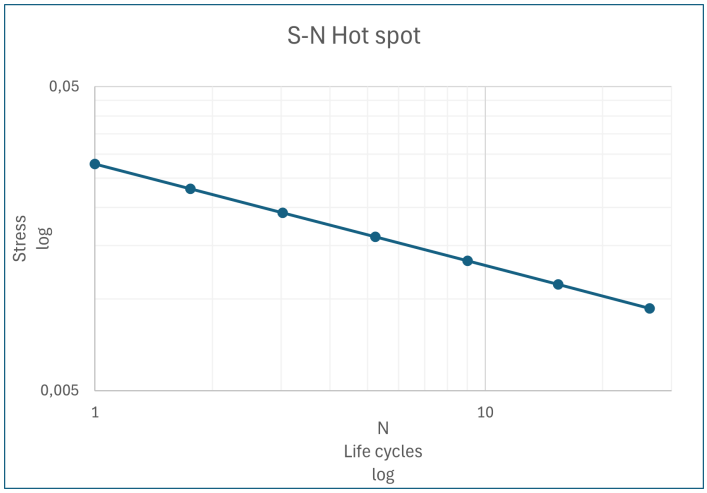

(b) Calculated S-N curve for the hot spot method.

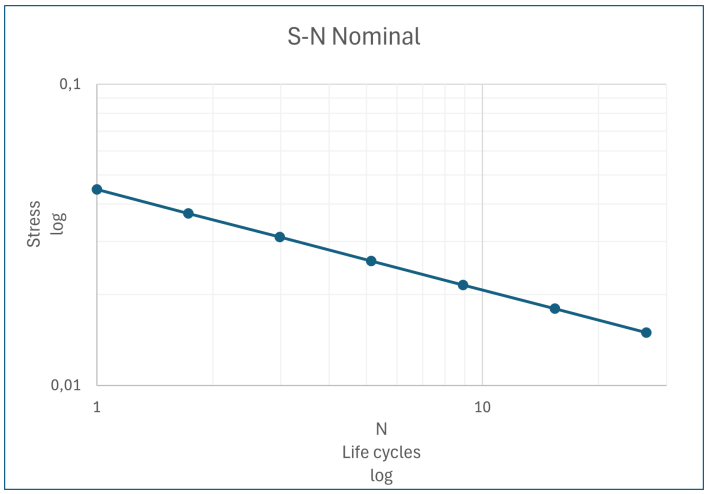

(c) Calculated S-N curve for the nominal method.

Figure 4.2: Normalized S–N curves for the different fatigue evaluation methods used in the study for Load System B. The curves are based on the selected FAT classes and describes the relationship between stress and number of cycles to failure. The calculated values were then normalized using a constant.

4.3 Fatigue Life – Load System C

In Load System C, a vertical force was applied to the side link. The conveyor belt consists only of one side link and two rods. For this Load System, no experimental data were available. The analysis is therefore based on the effective notch and nominal stress methods. The nominal stresses were calculated analytically, whereas the effective notch stresses are evaluated using the finite element method in ANSYS. The evaluated stress and corresponding life cycle values are normalized and plotted on logarithmic axes. Figures 4.3a and 4.3b present the stress-life curves for the two different methods. Five different load steps were used.

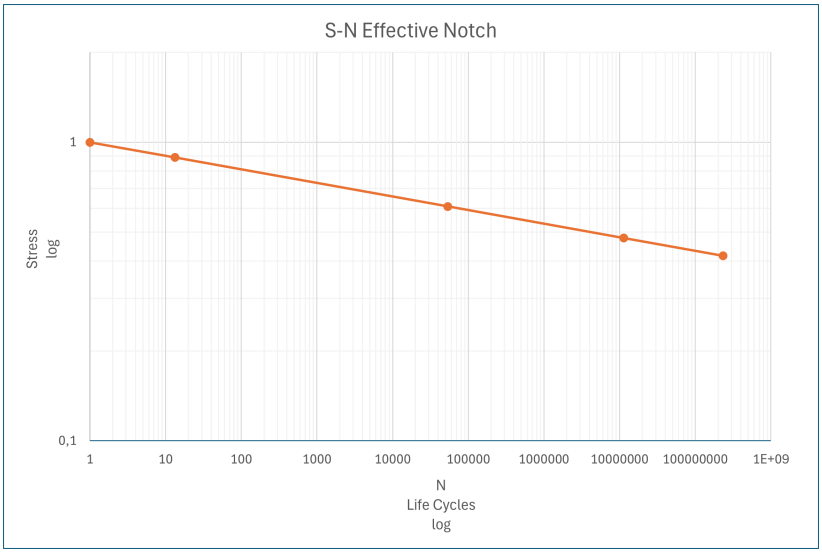

(a) Calculated S-N curve for the effective notch method.

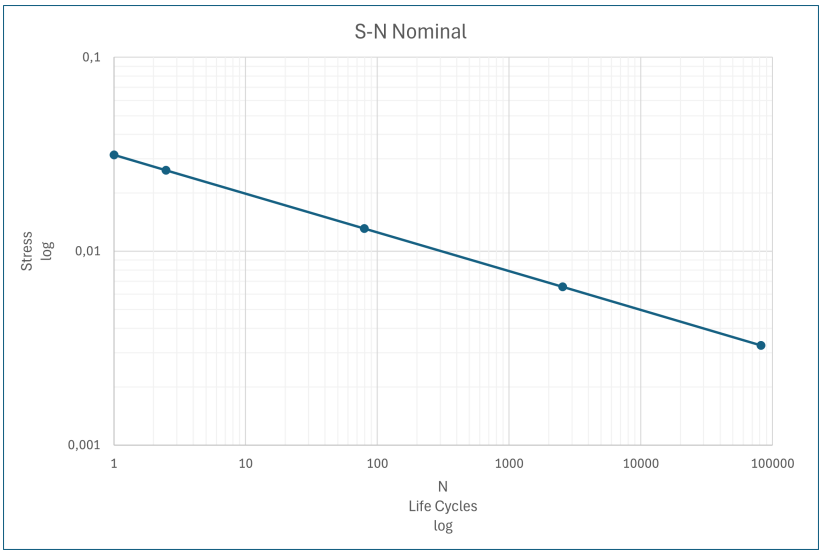

(b) Calculated S-N curve for the nominal method.

Figure 4.3: Normalized S–N curves for the different fatigue evaluation methods used in the study for Load System C. The curves are based on the selected FAT classes and describes the relationship between the stress and number of cycles to failure. The calculated values were then normalized using a constant.

4.4 Comparison of Load System A and B

Seven different load levels were used in the comparison between Load System A and B. The main differences between these Load Systems were the introduction of the tension link in Load System B. Nominal-, hot spot- and effective notch-stress methods were utilised in the evaluation.

For the effective notch stress method the comparison could be seen in Figure 4.4.

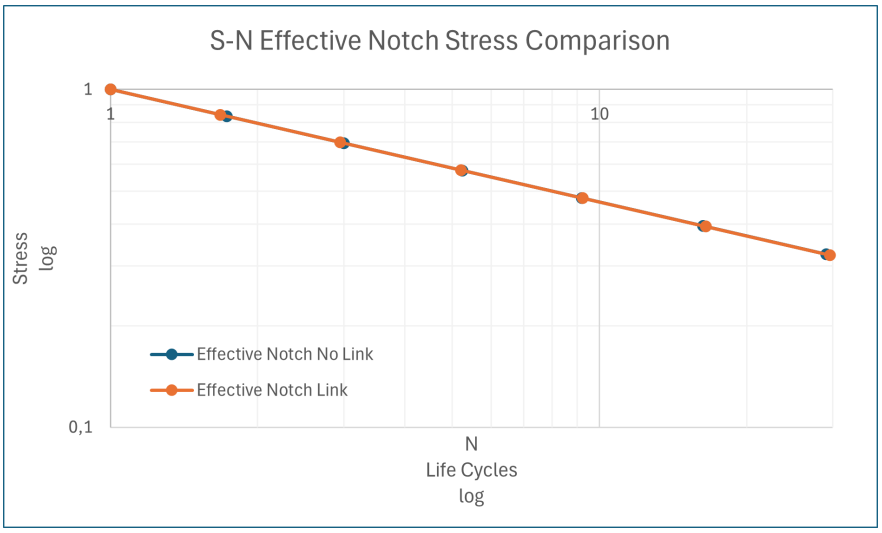

Figure 4.4: Comparison of normalised stress-life curves for Load Systems A and B using the effective notch method. Seven different load levels were evaluated to compare how the fatigue life changes between the two cases.

Figure 4.5 presents how the number of life cycles mostly increases when a tension link is introduced at the different load levels compared to without a tension link.

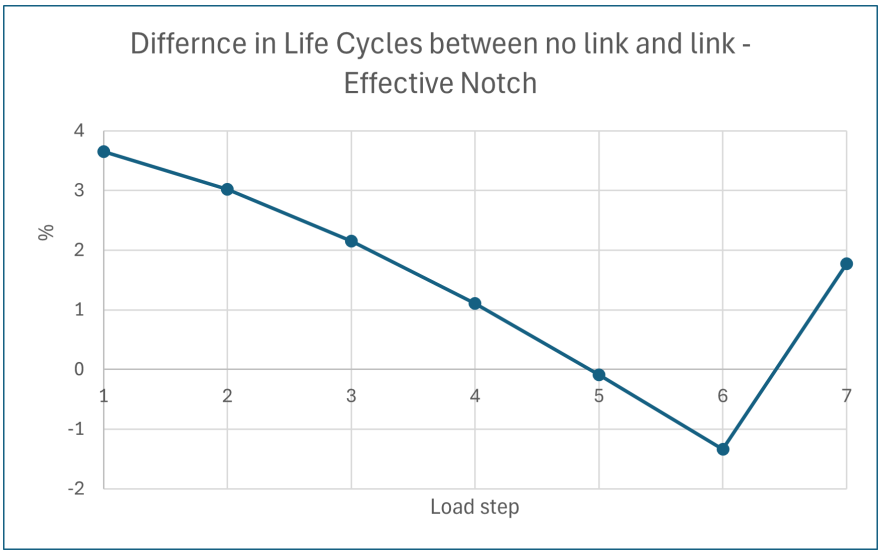

Figure 4.5: Increase in predicted life cycles for each load step after the introduction of the tension link in the conveyor system.

Then a comparison of the life cycles is made for the hot spot method, which could be seen in Figure 4.6.

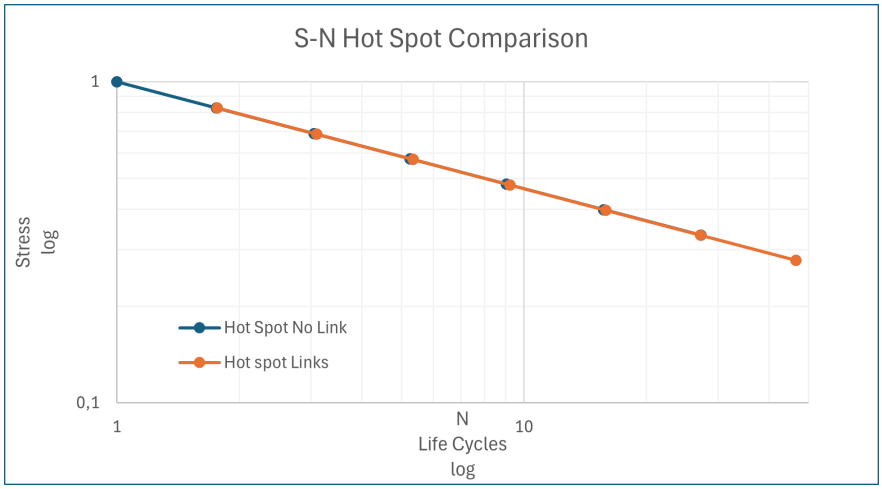

Figure 4.6: Comparison of normalised stress-life curves for Load Systems A and B using the hot spot method. Seven different load levels were evaluated to compare how the fatigue life changes between the two cases.

Once again, the percentage increase in the number of life cycles due to the tension link is analysed for each load step, this time using the hot spot method.

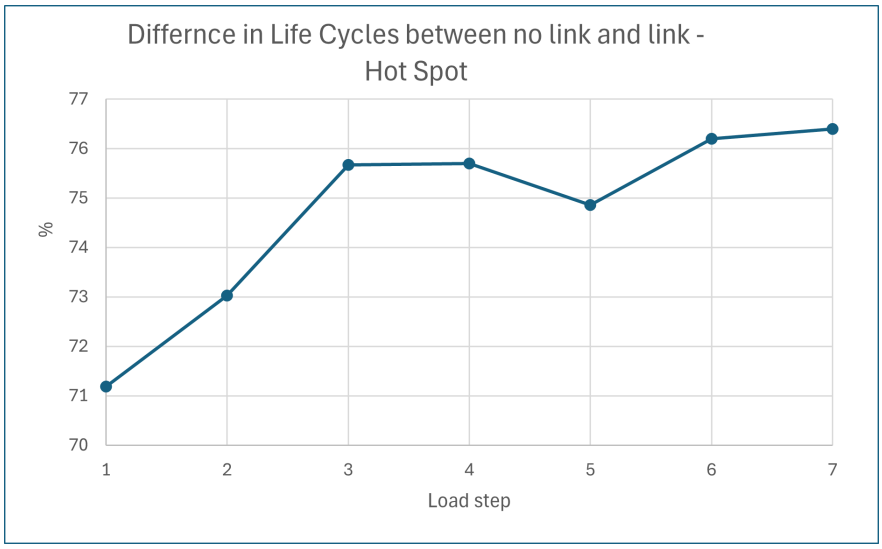

Figure 4.7: Increase in predicted life cycles for each load step after the introduction of the tension link in the conveyor system using the hot spot method.

A comparison of the life cycles for the nominal stress method is made and is seen in Figure 4.8

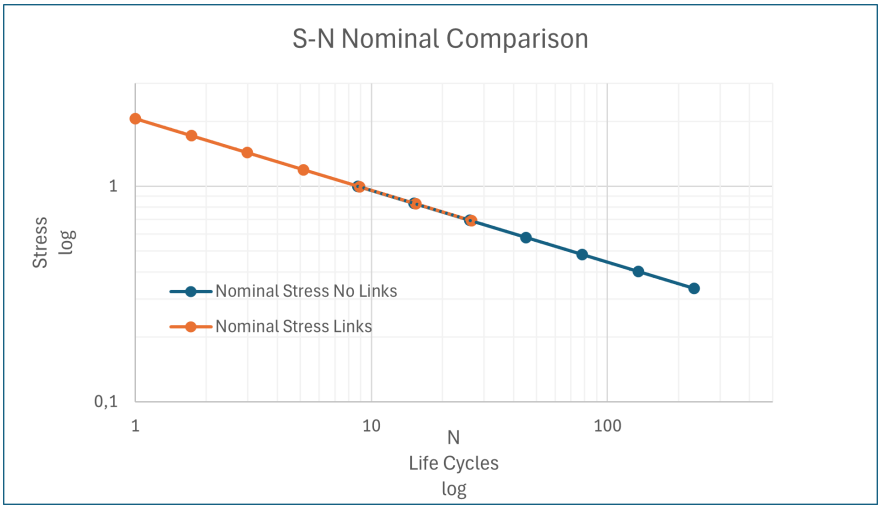

Figure 4.8: Comparison of normalised stress-life curves for Load Systems A and B using the nominal method. Seven different load levels were evaluated to compare how the fatigue life changes between the two cases.

Once again, it is analysed how many percent a tension link changes the number of life cycles at each load step. This time for the nominal stress method.

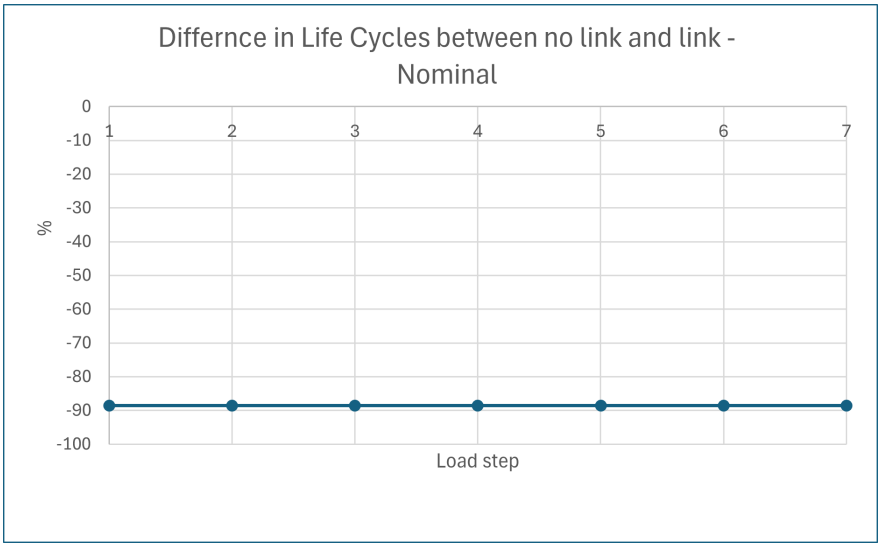

Figure 4.9: Reduction in predicted life cycles for each load step after the introduction of the tension link in the conveyor system using the nominal method.

4.5 Reduction Factor for Load System C

The reduction factor was then applied to Load System C and the figure below shows the reduction in fatigue life for each load step. The reduction factor was calculated using the effective notch stress method.

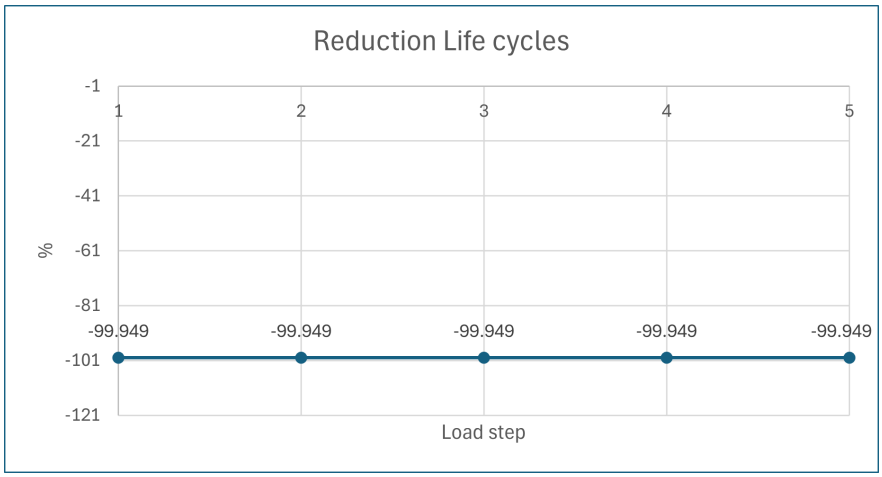

Figure 4.10: Reduction in predicted fatigue life for each load step after applying the reduction factor. The factor was implemented to Load System C to include stress variations from Load Systems A and B

4.6 Large Deflection – Load System B

When evaluating the stresses using the finite element program such as ANSYS, a comparison between analyses with large deflection activated and deactivated are presented in Figure 4.11. The results correspond to the stresses obtained at each load step for the respective analyses using the effective notch stress method.

Figure 4.11 shows marginally lower stress values when large deflection is activated. The difference increased slightly with increasing load step, although the overall variation remained small.

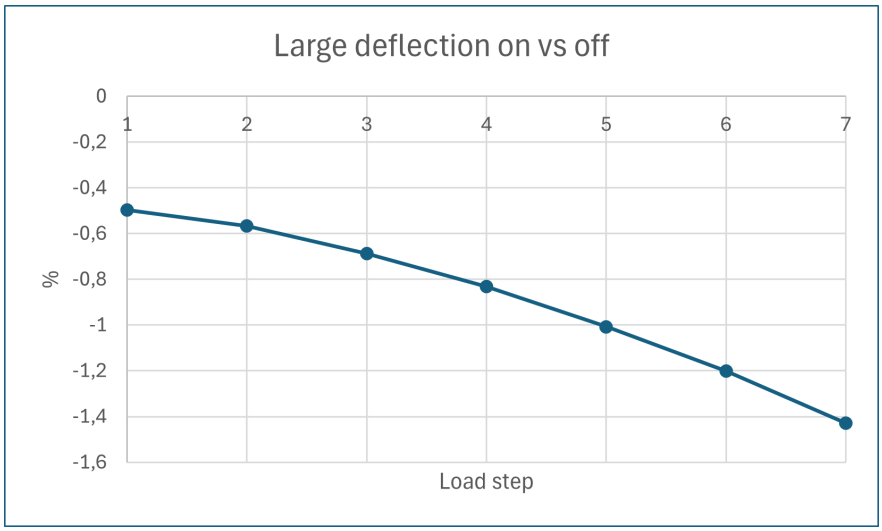

Figure 4.11: Percentage difference between the analyses performed with large deflection on and off. The comparison illustrates the influence of when large deflection is activated and the stiffness matrix is updated during the solution process to include geometric nonlinearity.

4.7 Parameter Study - Load System A

The parameter study was evaluated based on Load System A, where the maximum stress values were compared using the effective notch method. Load System A is the model without a tension link.

Figure 4.12 shows that the stress results differ depending on whether the weld size is reduced or increased. The weld throat dimension was increased and reduced by 0.5 mm relative to the original model.

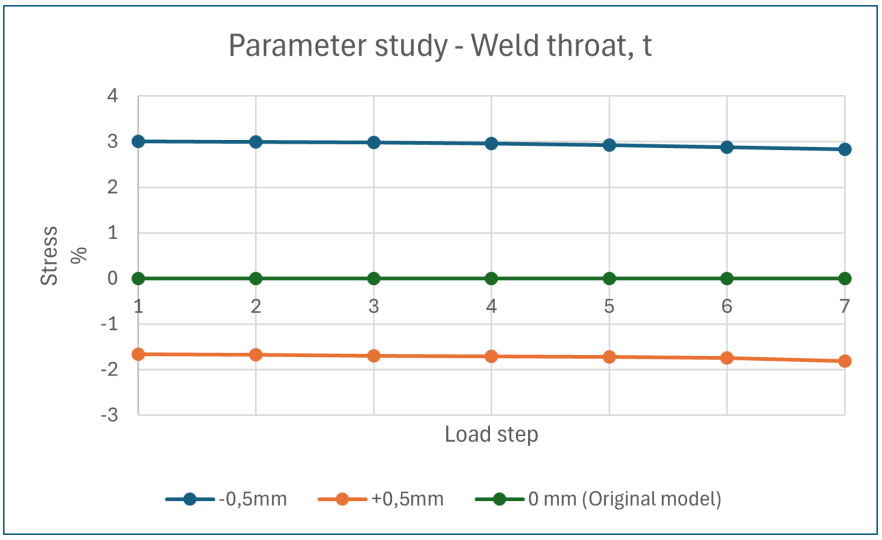

Figure 4.12: Percentage difference in the predicted stress levels between three different weld throat values. Illustrating how variations in weld size influence the local stress distribution

Figure 4.12 shows that an increased weld throat thickness reduced the stress by approximately 1,66%, whereas a decreased weld throat thickness increased the stress by about 3%.

4.8 Comparison between Large Deflection and Bi-linear isotropic hardening – Load System B

In Figure 4.13 and 4.14 a difference was observed between the result when large deflection is turned on or off compared to the Bilinear isotropic hardening results. The compared results are the stresses at three load steps. For both cases, the bilinear isotropic hardening model resulted in higher stresses in the weld compared to the two other models, regardless of whether large deflection is enabled or not.

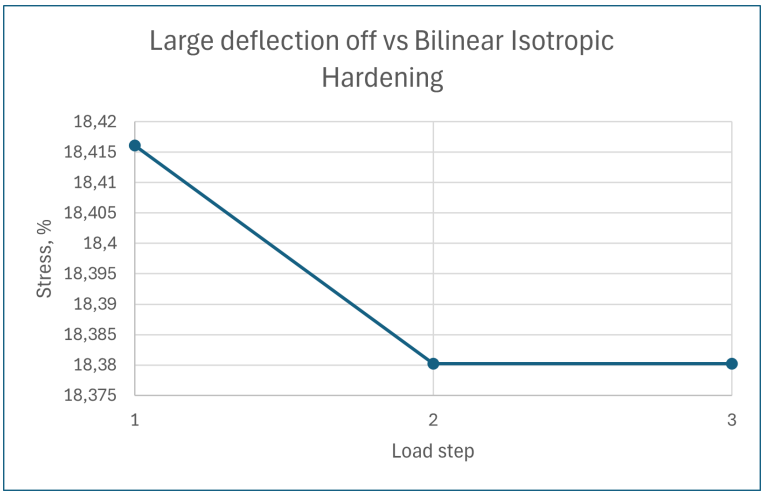

Figure 4.13: Percentage difference between linear elastic analysis with large deflection turned off and the Bi-linear isotropic hardening analysis for Load System B. The comparison show how material nonlinearity influences the predicted stress at three load levels.

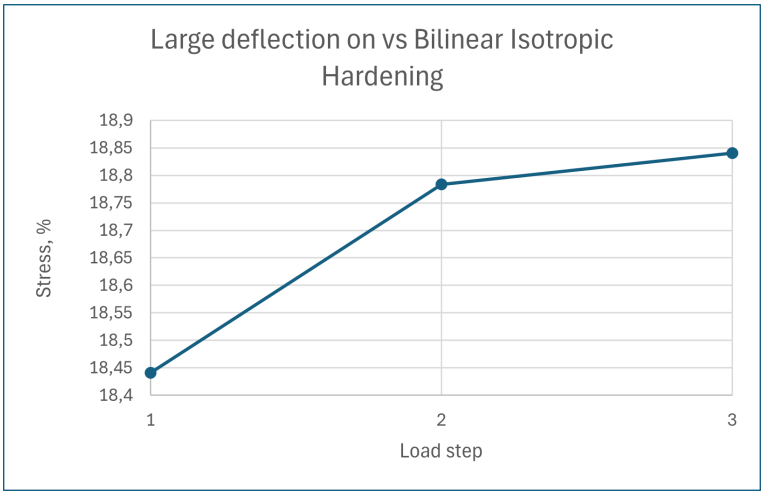

Figure 4.14: Percentage difference between linear-elastic analysis with large deflection turned on and the bilinear isotropic hardening analysis for Load System B. The comparison shows how material nonlinearity influenced the predicted stress at three load levels.

The difference between the bilinear elastic hardening model and the large deflection analysis, both on and of was approximately 18% at the fist load step. For load step two and three, small variations in the predicted stresses were observed when comparing

the two analyses., also as can be seen, the stresses are higher when large deflection is on.

5 Discussion

In this chapter, the results of the fatigue life assessment are discussed and evaluated. The differences between the evaluation methods are analysed, together with the influence of different load systems, modeling assumptions, and structural modifications such as the introduction of the tension link.

In reality, there are several factors that cannot be considered in finite element models. In the finite element analysis, a perfect weld geometry is assumed. However, in reality, perfect geometry does not exist, and welds produced during manufacturing cannot be guaranteed to be flawless or identical. Residual stresses are also present in real welded structures but were not included in the finite element models. Therefore, complete agreement between the numerical results and the real behaviour of the structure is difficult to achieve because fatigue performance in welded joints is influenced by several uncertainties.

5.1 Load System A & B

Load System A considers the belt without the tension link, while Load System B includes it. Both systems consider horizontal loading.

When comparing how close the different methods, effective notch, hot spot and nominal stress are to the actual test data, a certain spread in the results presented in the Tables 4.2 and 4.3 can be observed. These differences in results are not unexpected. The different methods are based on different theoretical assumptions and capture different parts of the stress field for the weld. The results from the different methods should therefore be seen as complementary approaches to the same load system for the two different Load Systems A and B. The different methods assess fatigue from different perspectives such as local peak stresses, structural stresses, and global nominal stresses.

The effective-notch was developed to capture local peak stresses and therefore requires a very fine mesh in order to provide reliable results. Since the method represents a local assessment of fatigue risk, small variations in the mesh may generate large differences in the results. In tables 4.2 and 4.3 it can be seen that this method is significantly further away from the aim value, compared with the other two evaluation methods. When comparing Figure 4.1a with 4.1b and 4.2c, it can be seen that the effective notch method has a significantly shorter lifetime than the other two evaluation methods. The method generates very high local stress peaks at the radius, which can cause the predicted fatigue life to be shorter, compared to the other two methods. For loading scenarios dominated by shear stresses, as in Load Systems A and B, no explicit assessment approach is provided in [20]. Existing methods are primarily developed for loading conditions where the stress component acts perpendicular to the weld. In cases where the loading is mainly parallel to the weld, it increases the sensitivity of

the evaluation and may lead to greater uncertainty in the results. Therefore, the use of these methods with dominant shear stresses remains limited, and a consistent and well-established procedure for such loading conditions is not clearly defined in the literature.

At high shear stresses, the effective notch method can become sensitive. This is relevant for the investigated load systems in question, since the stress states in these two cases are strongly dominated by shear stress acting parallel to the weld. The effective notch method is often expected to predict higher local stress levels than both the hot-spot and nominal stress methods, especially when shear stresses are dominant. A contributing reason is that the method is based on a linear elastic assumption and does not allow plastic redistribution of stresses. As a result, local shear stress peaks are not being reduced and may instead be overestimated. For this reason, the effective notch method may therefore be questionable for load systems with large shear dominated stresses parallel to the weld according to [20].

The hot spot method is primarily intended to describe the structural stress increase close to the weld. The method is based on extrapolation of stresses obtained from the finite element analysis at specified distances from the weld. As a result, the hot spot captures the global and local effects of load variations, plate thickness and stiffness variations. Therefore, the hot spot method does not generate the same extreme local stress peak that the effective notch method generates. As can be seen in Table 4.2 and 4.3, the hot spot method results are located between the effective notch and nominal stress results.

A possible reason is that the hot spot method is based on extrapolation of stresses evaluated at specified distances near the weld. Because of this, the method becomes less sensitive to local stress peaks in the weld compared to the effective notch method. This results in a lower stress gradient and lower stress values, which in this case show better agreement with the test results.

In [20] it is explained that the hot spot method is defined for stresses acting perpendicular to the weld. Other stress directions, such as loading parallel to the weld, need to be treated differently and are not directly included in the method. Unfortunately, there are limited data and guidance for such loading cases. As observed in this study, this can reduce the reliability of the results when the load is dominated by shear stresses.

The nominal stress method is the most simplified evaluation approach. Since it assumes only a global load distribution, it does not capture local stress concentrations that influence the fatigue behaviour. As shown in Table 4.2 and 4.3 this method predicts the lowest values. Local geometric variations are therefore not included in the analysis, causing the nominal stress to remain constant and potentially lower than the actual stress state.

In Load System B, the nominal stress method shows the closest agreement with the experimental test data. In reality, the load is distributed between both the side link and the tension link. However, in the nominal stress method, the tension link is assumed to carry the entire load. If load redistribution was considered, the stress

in the weld would decrease, resulting in an increased fatigue life. As a result, the percentage for the nominal stress method in Table 4.3 would likely be reduced more. However, no analysis of the nominal stress method including load redistribution was performed. The magnitude of this effect is therefore unknown.

In summary, the results of the three different methods show that they capture different parts of the stress field. As a result, identical results from all methods should not be expected. The effective notch captures the local peak stresses, hot spot the structural stress increase and the nominal stress describes the global stress distribution. The difference in the results is therefore reasonable and reflects the purpose of each evaluation method.

5.2 Load System C

For Load System C, no experimental data were available for validation. Therefore, the fatigue assessment is based on the nominal stress method and the effective notch stress method. In this load system, the belt is subjected to vertical loading, which produces a different stress distribution compared to the other load systems and thereby influences the predicted fatigue life differently.

As shown in Figure 4.3b, the nominal stress approach predicts a lower fatigue life during the first two load steps. This indicates that, at relatively high load levels, the nominal stress method provides a more conservative estimate of fatigue life than the effective notch stress method. One possible explanation is that the nominal stress method does not explicitly account for local stress redistribution at the notch in the same way as the effective notch stress method does. Instead, it evaluates the fatigue strength based on a structural stress level, which may lead to a lower predicted fatigue life.

Since no experimental data are available for Load System C, it is not possible to determine which method predicts the most accurate prediction. Although no experimental data are available, the comparison is still useful because it highlights the methodological differences between the two approaches. The results indicate that the predicted fatigue performance depends strongly on the selected fatigue assessment method. The nominal stress and effective notch stress methods evaluate the stress state differently, which may lead to different fatigue life predictions for vertically loaded belt conditions. The results should therefore be reviewed with caution when comparing methods.

5.3 Comparison Between Load Systems A & B

Figures 4.4 and 4.5 show only minor differences in both stress levels and the fatigue life for the effective notch method. Load System A and Load System B produce almost identical results. The introduction of the tension link increases the fatigue life by a couple of percent and then decreases until load step 6 before increasing again in load step 7. This may be due to the load being redistributed during the different load steps. Since the difference is so small it does not necessarily indicate an error in the model. Instead, the behaviour may reflect variations in how the load is transferred through the conveyor belt during different loading stages.

In the hot spot method, shown in Figure 4.6 and 4.7, a similar behaviour can again be observed. However, a greater variation in the result is obtained when the tension link is introduced. When comparing the fatigue life in Figure 4.7, a more noticeable difference between the two load systems can be observed. The fatigue life increases by over 70% when the tension link is introduced. A small reduction in fatigue life is again observed at load step 5 but then increases again at load step 6 and 7. This trend is similar to the one observed for the effective notch stress evaluation method.

When comparing the results of nominal stress in Figure 4.8 and 4.9 the largest variations in the results can be seen. This is particularly seen in Figure 4.9 where the introduction of the tension link appears to reduce the fatigue life, rather than improve it. One possible explanation is that the nominal stress only captures the global effects. Many local effects that are important in fatigue analysis are therefore not captured. As a result, the predicted behaviour may not fully reflect reality, since large stress variations are not included.

5.4 Reduction Factor for Load System C

The reduction factor calculated for Load System A using the effective notch stress approach is relatively large, as seen in Figure 4.10. However, the primary purpose of the reduction factor is to account for any imperfections or stress levels in the weld that are not captured in Load System C. Despite the substantial reduction, the resulting life cycles remain high. The reduced fatigue life is therefore considered a more representative estimate than the fatigue life calculated using the finite element method alone for Load System C without a reduction factor.

5.5 Large Deflection Comparison - Load System B

As shown in Figure 4.11, activation of large deflection results in a small difference in the stress levels. A reduction of 1% means that no large rotations, deformations or load path change when the stiffness matrix is being updated.

The stresses in the model are mainly dominated by local geometries and stress con-

centrations instead of large global deformations or rotations. Therefore, the results are only marginally affected when activating large deflection.

5.6 Parameter Study - Load System A

In the parameter study, two different weld sizes were investigated and compared with the original weld size. As shown in Figure 4.12, an increase of 0.5 mm in the weld throat resulted in approximately 1.7–1.8% reduction of the stress. These results indicate that a larger weld size improves the fatigue life of the conveyor belt. In contrast, reducing the weld throat by 0.5 mm led to an increase in stress of approximately 3 %. This result is consistent with the theory that a smaller cross-sectional area results in higher stress in the weld, which in turn reduces the number of load cycles the whole belt can withstand.

5.7 Comparison between Large Deflection and Bilinear Isotropic Hardening – Load System B

In figures 4.13 and 4.14 show that the stresses based on the deformations obtained from the bilinear isotropic hardening analysis are higher than those from a completely linear elastic analysis. The bilinear model is first performed to capture the structural deformation and these deformations are then used as the basis for a new linear stress analysis.

This result is expected because when the material is modeled with bilinear isotropic hardening plastic deformations occur. These plastic displacements and rotations mean that the structure is already in a more unfavourable deformed state when the linear calculation is carried out. The changed geometry affects the load paths and therefore increase the stress levels in the weld.

The stress increase is approximately 18% for both comparisons with the completely linear elastic analysis. Since the difference between the cases with and without large deflection is so small, the result shows that the dominant cause of the stress increase is the plastic deformation introduced by the bilinear isotropic hardening model, as seen in 4.13 and 4.14. Large deflection therefore only affects the results very little when the comparison is made between theses two figures.

6 Conclusions and Future Studies

6.1 Conclusions

6.1.1 Overall Conclusions

Based on the comparison between experimental tests and the stress distributions of the finite element analysis, the hot spot stress method is recommended for practical fatigue assessment of the conveyor belt welds. The effective notch method is more suitable for detailed investigations of local weld geometry together with stress concentrations. The nominal stress method can provide a fast and simplified overview of the global stress beheaviour and quickly generate the fatigue performance of the weld.

By increasing the weld throat thickness it improves the fatigue life of the conveyor belt by reducing the stresses in the weld. However, larger welds also increase material cost and manufacturing time. In return, this may lead to stricter inspection requirements. A larger weld contains more material and therefore has a higher risk of weld defects. The increased heat input and longer welding time can also affect the stresses in the weld.

6.1.2 Case study Findings

For Load Systems A and B, the investigated weld was identified as one of the critical regions due to the high stresses observed in the finite element analysis. The stresses were mainly dominated by shear stresses, although tensile stresses were also present, since the conveyor belt was loaded parallel to the weld. The introduction of the tension link redistributed the load within the structure and reduced the stress level in the investigated weld. The results indicate that the tension link influenced the overall stress distribution in the conveyor belt structure.

6.1.3 Findings Related to FEM and Modeling Approaches

When modelling the effective notch method, which is one of the more demanding evaluation methods, it was difficult to achieve a smooth stress distribution between the weld and the side link. Small radii and semi-circular geometries over thin cross-sections were challenging to model accurately and sometimes introduced stress peaks caused by modeling imperfections. These stress concentrations were reduced by refining the geometry and adding suitable radii in critical regions. Compared with the effective notch the hot spot method was less demanding from a modeling perspective since fixed evaluation points were defined for stress extraction.

The large deflection analysis had only a minor impact on the results. This indicates

that the local weld geometry and stress concentrations have a greater impact on fatigue life than the global deformation and rotations.

The bilinear isotropic hardening model was first performed to capture the plastic deformations and was then used as the starting point for a linear analysis. This resulted in higher stresses than the fully linear elastic model without plastic deformations as a starting point. This means that material nonlinearity can influence the stress distribution and fatigue life estimations of welded structures.

6.1.4 Findings Related to different Fatigue Analysis methods

It was observed that the welds loaded parallel to the weld direction created a more complex stress field that made the fatigue evaluation more difficult. As a result, the different fatigue evaluation methods produced significantly different results. For hot spot and nominal stress methods, it was also necessary to identify a suitable weld category for the calculations. In this study, there was no weld category that perfectly matched the evaluated weld geometry, so the closest suitable category had to be selected for the calculations.

For load systems where the welds were loaded perpendicular to the weld direction, the evaluation methods produced more consistent results. This indicates that limitations exist in the Eurocode and other fatigue evaluation methods when assessing welds subjected to loading parallel to the weld direction, which may be attributed to substantial uncertainties.

6.1.5 Industrial Relevance

The findings of this study will provide a better understanding of how different weld evaluation methods describe the fatigue behaviour of the conveyor belt welds. The results can support JBT Marel in future work with design improvements, weld optimisation and selection of suitable assessment methods for fatigue in conveyor belt applications.

6.1.6 Conclusion Based on the Research Objectives

- How does the introduction of a tension link affect the load distribution within the conveyor belt structure?

The introduction of a tension link affects the load distribution within the conveyor belt. The magnitude of this effect depends on the stress assessment applied. Both the hot spot and effective notch stress methods show a reduction in the stress concentrations. In contrast, the nominal stress method predicts an increase in stress. However, the nominal stress method only captures the global load distribution and does not account for local effects. In comparison, the effective notch method captures the local stress and hot spot stress methods capture both global and local effects of the load variations.

The nominal stress method has assumed that the entire load is transferred through the tension link but in reality there will be a distribution between tension link and side link. This means that the results obtained using this method do not correspond to the same tendencies as the effective notch and hot spot method. However the nominal stress method still provides a reasonable indication of the global load distribution within the structure.

- To what extent do numerical fatigue life estimations correlate with simplified fatigue tests performed on the conveyor belts?

The numerical fatigue life estimations show a certain degree of correlation with the experimental tests performed on the conveyor system. However, the level of agreement is strongly dependent on the numerical method applied, as different approaches capture the stress distribution and fatigue behaviour with varying levels of accuracy. In this case, the nominal- and hot spot stress methods show closer agreement with the experimental results, indicating that they provide a more representative description of the structural behaviour under the given loading conditions.

- How does the thickness of the weld affect the fatigue life estimations?

The results indicate that the thickness of the weld has a influence on the fatigue life estimations. An increase in weld thickness leads to a more favourable stress distribution and reduced stress concentrations, which contribute to an extended fatigue life. This has been observed using the effective notch stress method.

6.2 Future Studies

- Perform fatigue testing for other load systems. Testing additional load systems could provide a broader understanding of the stress concentrations and the fatigue behaviour. It could also help validate the results presented in this study.

- Validate load sharing between side link and the tension link using strain gauges. Such tests would provide a better understanding of how the load is distributed between the side link and the tension link.

- Including residual stresses, weld imperfections and temperature variations in the analysis. Including these effects could make the study more realistic. Residual stresses near the weld could increase the local stress concentrations. Introducing weld imperfections would also provide a more realistic representation of the weld geometry, since a perfectly manufactured weld cannot always be guaranteed in practice. Temperature variations could influence the material behaviour because the conveyor belt is exposed to changing temperatures while passing through the machine. These effects may in turn influence the fatigue life of the welded joints.

- Investigate how increasing the diameter of the rod affects the weld. A larger rod diameter could change the stiffness of the connection and change the stress distribution around the weld. This could either reduce or increase the local stress concentrations depending on how the load is transferred between the rod, weld and side link. A study like this could provide a better understanding of whether an increased rod diameter would improve the fatigue life of the welded joint. It could also provide useful guidance for future design improvements of the conveyor belt.

- Analyse how the stress in the weld changes if the weld is moved slightly away from the eccentric position on the rod. Changing the weld position could affect how the load is transferred between rod, weld and side link. This could either reduce or increase the local stress concentrations in the weld. Such an investigation could improve the understanding of how small deviations in the weld position affect the stress distribution and fatigue results, since a exact weld location cannot always be guaranteed during manufacturing.

Bibliography

[1] Qingyuan Wang, Shun-Peng Zhu, José Correia, Abílio De Jesus and Grzegorz Lesiuk. *Fatigue of Materials and Structures: Physics and Data Science. [Elektronisk resurs]*. CRC Press, 2025.

[2] Wei Zhang. "Technical Problem Identification for the Failures of the Liberty Ships." In: *Challenges (20781547)* 7.2 (2016), p. 20.

[3] Mohammad Al-Emrani and Björn Åkesson. *Steel Structures*. Gothenburg, Sweden: Chalmers University of Technology, 2018.

[4] S. Suresh. *Fatigue of materials.* Cambridge ; New York: Cambridge University Press, 1998.

[5] D Radaj. *Design and Analysis of Fatigue Resistant Welded Structures.* Woodhead Publishing, 1990.

[6] C. Constantineau, P.A. Deschênes, R. Dubois and M. Brochu. "Fatigue strength prediction of 410NiMo stainless steel with surrogate weld discontinuities". In: *International Journal of Fatigue* 197 (2025).

[7] Gary B. Marquis, Zuheir Barsoum and Series editor IIW International Institute of Welding. "IIW Recommendations on High Frequency Mechanical Impact (HFMI) Treatment for Improving the Fatigue Strength of Welded Joints". In: *IIW Recommendations for the HFMI Treatment : For Improving the Fatigue Strength of Welded Joints* (2016), pp. 1–34.

[8] Abinab Niraula and Heikki Remes. "The severity of local undercut on fatigue life of welded joints". In: *International Journal of Fatigue* 197 (2025).

[9] Zhengping He, Bingzhi Chen, Xiangwei Li, Xv Zhang, Jianxin Xv and Shangchao Zhao. "Notch effect identification and fatigue life prediction of undercut weld". In: *Engineering Fracture Mechanics* 294 (2023).

[10] M.J. Ottersböck, M. Leitner and M. Stoschka. "Characterisation of actual weld geometry and stress concentration of butt welds exhibiting local undercuts". In: *Engineering Structures* 240 (2021).

[11] "IIW Recommendations for the Fatigue Assessment of Welded Structures by Notch Stress Analysis: IIW-2006-09". In: *IIW Recommendations for the Fatigue Assessment of Welded Structures by Notch Stress Analysis* (2012), p. 2.

[12] J. Schijve. *Fatigue of Structures and Materials.* Dordrecht : Springer Netherlands : Imprint: Springer, 2009.

[13] Mohammad Al-Emrani and Mustafa Aygül. *Fatigue Design of Steel and Composite Bridges*. Report 2014:10. Göteborg, Sweden: Chalmers University of Technology, Department of Civil, Environmental Engineering, Division of Structural Engineering, Steel and Timber Structures, 2014.

[14] Anastasios P. Vassilopoulos and Thomas Keller. *Fatigue of Fiber-reinforced Composites.* London : Springer London : Imprint: Springer, 2011.

[15] author Anand Lallit, author Kamrin Ken and author Govindjee Sanjay. "Fatigue". In: *Introduction to Mechanics of Solid Materials* (2022).

[16] Tatsuo Endo and Y. Murakami. *The rainflow method in fatigue. the Tatsuo Endo memorial volume : the papers presented at the International Symposium on Fatigue Damage Measurement and Evaluation Under Complex Loadings in memory of Prof. Tatsuo Endo, the inventor of the rainbow method, Fukuoka, Japan, July 25-26, 1991, supported by ONO SOKKI Co. Ltd.* Oxford ; Boston: Butterworth-Heinemann, 1992.

[17] Hong Zhang, Lei Shi, Xuhui Liu, Xianshu Leng, Ding Feng and Paul Tu. "Research on the spindle deflecting reliability of the wellbore trajectory control tool based on Palmgren-Miner". In: *Journal of Mechanical Science and Technology* 34.12 (2020), pp. 4925–4931.

[18] Yuege Zhou, Dingyun Liu, Dandan Li, Yan Zhao and Weifang Zhang. "Thermal Fatigue Life Prediction for Optical Fibers Based on Nominal Stress Method". In: *2020 Prognostics and Health Management Conference (PHM-Besançon), Prognostics and Health Management Conference (PHM-Besançon), 2020, PHM-BESANCON* (2020), pp. 103–108.

[19] Erkki Niemi, Wolfgang Fricke and Stephen J. Maddox. *Structural Hot-Spot Stress Approach to Fatigue Analysis of Welded Components: Designer's Guide. [Elektronisk resurs]*. Springer, 2018.

[20] A. F. Hobbacher. *Recommendations for Fatigue Design of Welded Joints and Components: IIW Document IIW-2259-I5 Ex XIII-2460-13/XV-1440-13. [Elektronisk resurs]*. Springer International Publishing, 2016.

[21] Bertil Jonsson, G. Dobmann, A. F. Hobbacher, M. Kassner, G. Marquis and Series editor Mayer Cécile. "IIW Fatigue Assessment Procedures". In: *IIW Guidelines on Weld Quality in Relationship to Fatigue Strength* (2016), pp. 11–18.

[22] European Committee for Standardization. *Eurocode 3: Design of Steel Structures – Part 1-14: Fatigue*. Brussels, Belgium: CEN, 2023.

[23] Nilesh Singh Avinash Datarkard Amruta Pasarkar Atish Mane and Nilesh Raut. *A Review of Fatigue Behaviour of Resistance Spot Welds preventers*. Report. Laval, Pune: Bharati Vidyapeeth's College of Engineering, 2022.

[24] Ibrahim T. Teke and Ahmet H. Ertas. "Fatigue Testing and Life Prediction of Tensile Shear Spot-Welded Joints: A Comprehensive Review with Regression Modeling". In: *Iranian Journal of Science and Technology, Transactions of Mechanical Engineering* 49.4 (2025), pp. 1619–1647.

[25] Ilyas Kacar and Sefa Yildirim. "Parameter Calibration of a Novel Combined Hardening Model for a Wire Drawing Simulation of AA7075-T6". In: *Journal of Materials Engineering and Performance* 34.10 (2025), pp. 8691–8706.

[26] European Committee for Standardization. *Eurocode 3: Design of Steel Structures – Part 1-9: Fatigue*. Brussels, Belgium: CEN, 2023.

[27] Niels S. Ottosen and Hans Petersson. *Introduction to the Finite Element Method*. Pearson Education, 1992.